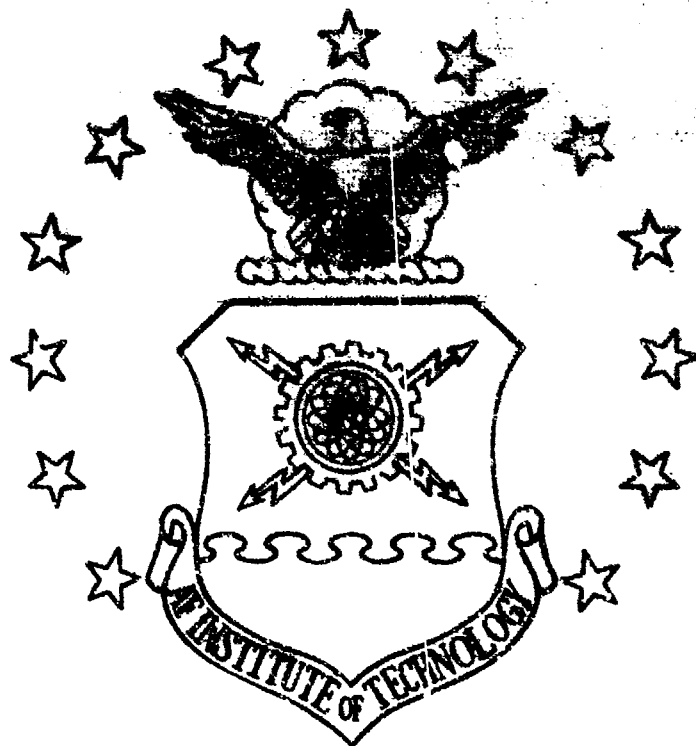


AD A 136895



A STUDY OF THE AERODYNAMIC INTERFERENCE
EFFECTS DURING AERIAL REFUELING

THESIS

Eric H. Hoganson
Captain USAF

AFIT/GAE/AA/330-8

DTIC
ELECTIC
JAN 18 1984

This document has been approved
for public release in its entirety.
Distribution is unlimited.

DEPARTMENT OF THE AIR FORCE
AIR UNIVERSITY

AIR FORCE INSTITUTE OF TECHNOLOGY

Wright-Patterson Air Force Base, Ohio

84 01 17 132

AFIT/GAE/AA/83D-8

①

A STUDY OF THE AERODYNAMIC INTERFERENCE
EFFECTS DURING AERIAL REFUELING

THESIS

Eric H. Hoganson
Captain USAF

AFIT/GAE/AA/83D-8

SECRET
ELECTRICAL
JAN 18 1964
A

Approved for public release; distribution unlimited

AFIT/GAE/AA/83D-8

A STUDY OF THE AERODYNAMIC INTERFERENCE
EFFECTS DURING AERIAL REFUELING

THESIS

Presented to the Faculty of the School of Engineering
of the Air Force Institute of Technology

Air University

In Partial Fulfillment of the
Requirements for the Degree of
Master of Science in Aeronautical Engineering

Eric H. Hoganson, B.S.

Captain, USAF

December 1983



Distribution/	
Availability Codes	
Dist	Avail and/or Special
A-1	

Approved for public release; distribution unlimited

Preface

One of the major reasons I selected this topic was my background as a B-52 receiver pilot. Throughout the study I tried to use my flying experience to provide a little more insight to what really happens behind a tanker. As a Flight Instructor, I am also aware of some of the problems students have when learning how to air refuel. This knowledge enabled me to choose some of the areas I emphasized in the report. To date, little has been published on air-refueling aerodynamics and I hope this report can help stimulate more interest in the subject.

This effort would not have been possible without the help of a number of people. I would first like to thank the members of my thesis committee, Major Eric Jumper and Captain Hugh Briggs, for their help in this undertaking. I would also like to thank my thesis advisor Lt Col Michael Smith whose patience and direction were essential in completing my thesis. Lt Marc Masquelier, Rimentas Liaugminas, Ojars Skujins, and William McClure sponsored the project and their aid was very much appreciated. A special thanks to Mr. James Snyder who gave me the Latex program and helped me get it working on the AFIT computer. Finally a big thank you to my wife Tawnie and my daughter Bethany whose love and support kept me going throughout the project.

Eric H. Hoganson

Table of Contents

	<u>Page</u>
Preface	ii
List of Figures	v
Notation.	vii
Abstract.	viii ix
I. Introduction	1
Background.	1
Purpose	2
Approach.	3
Result Summary.	5
II. Air Refueling - A Receiver Pilot's Perspective.	6
III. Analytical Approach.	9
Method 1 - Tent Circulation Distribution.	12
Method 2 - Modified Linear Circulation Distribution.	14
Method 3 - Horse Shoe Vortex Circulation Distribution.	15
Compressibility Considerations.	20
IV. Vortex Lattice Method.	21
V. Results.	27
Analytical Results.	28
VLM Results	33
VI. Conclusions and Recommendations.	49
Appendix A: Velocity Field Induced by a Linear Lifting Line and a Semi-Infinite Sheet at any Point in Space.	52
Appendix B: Comparison of Gamma of Elliptical Lift Distribution and Linear Lift Distributions.	65
Appendix C: Operation of the LATEX Program	68

	<u>Page</u>
Appendix D: Relationship of Aerodynamic Coefficients and Circulation (VLM)	81
Bibliography.	84
Vita.	86

List of Figures

<u>Figure</u>		<u>Page</u>
1	Tent Circulation Distribution	4
2	Modified Linear Circulation Distribution.	4
3	Horse Shoe Vortex Lift Distribution	4
4	Receiver Approach Path in Relation to the Location of the Tanker Tip Vortices	11
5	Sketch of Assumed Tanker Wing (Coordinate system.	13
6	Sketch of a Horse Shoe Vortex Modeling the Tanker.	16
7	Vortex Lattice Panelled Wing.	21
8	Refueling Coordinate System (Vortex Lattice Method)	24
9	Analytical Downwash Versus Span Location (Contact Position) KC-10 $W+=590,000$ lbs	29
10	Analytical Downwash Versus Span Location (Contact Position) KC-10 $W+=260,000$ lbs	30
11	Analytical Downwash Versus Span Location (Contact Position) $W+=260,000$ lbs	31
12	Analytical Downwash Versus Span Location (Precontact Position) $W+=260,000$ lbs.	32
13	B-52 C_L Versus Alpha Curve.	34
14	KC-10 C_L Versus Alpha Curve	34
15	VLM Downwash Comparison (at the B-52 wing) of Rectangular and Swept Tanker Wings	35
16	KC-10 Sectional Lift Coefficient Versus Span (VLM).	37
17	VLM Induced Downwash Velocity Versus Span Position	38

		<u>Page</u>
18	VLM Induced Downwash Velocity Versus Span Position (x=525 ft, z=75 ft)	39
19	Induced Downwash Velocity Versus Span Position (Precontact Position).	40
20	Induced Downwash Velocity Versus Span Position (Contact Position)	41
21	Induced Downwash Velocity Versus Span Position (Contact Position)	42
22	Induced Upwash Velocity on the KC-10 Caused by the B-52.	44
23	Change of KC-10 Lift Coefficient Versus B-52 Position	45
24	B-52 Positions Evaluated by VLM	47
25	Change of B-52 Angle of Attack Versus B-52 Position	48
26	Change of B-52 Pitching Moment Coefficient Versus B-52 Position.	48
27	Sketch of Assumed Tanker.	52
28	Tanker Represented by Tent Circulation Distribution.	57
29	Tanker Represented by Modified Linear Circulation Distribution.	60
30-32	LATEX Formating Information	69
33	LATEX Sample Input File	72
34	Paneling Used on KC-10 Wing	74
35-38	Sample Output File.	77

Notation

A	Distance behind tanker lifting line
{A}	Influence coefficient matrix
α	Angle of attack
B	$(1 - M_\infty^2)^{\frac{1}{2}}$
b	Wing span
b'	Effective wing span
c	Chord length
C_L	Lift coefficient
C_M	Moment coefficient
Γ	Circulation strength
H	Distance below tanker lifting line
M	Mach number
N_s	Number of semi-span panels
$P(x,y,z)$	Point of interest
R	$x^2 + y^2 + z^2$
S	Wing area
U	Free stream velocity
u	Induced velocity in the x direction
V	Total induced velocity
v	Induced velocity in the y direction
V_d	Descent velocity of wing tip vortex pair
w	Induced velocity in the z direction
x	Distance behind the tanker wing in the direction of U

y

Spanwise distance off tanker centerline
(positive to the right)

z

Distance normal to tanker wing at zero
angle of attack (positive up)

Abstract

This report ^{investigated} ~~documents an investigation of~~ the feasibility of using an analytical approach and the vortex lattice method ^(VLM) ~~for the evaluation of~~ the aerodynamic interference effects present during aerial refueling.

^{While} A KC-10 tanker and a B-52 receiver were ~~selected for study~~ ^{however,} the method can be applied to any tanker and receiver combination. The major assumptions include: linear potential flow; tanker and receiver are represented by wing planforms; fuselage effects are small; and the rolling-up process of the tanker's wing tip vortices are not considered. The analytical approach uses a lifting line followed by a semi-infinite vortex sheet to represent the tanker. Three linear lift distributions for the tanker's wing were used and equations were derived for the induced downwash at any point in space. Points ~~were selected~~ ^{were selected} on the receiver's wing to indicate the tanker's effect on the receiver's flowfield. Results of the analytical equations ^{when} ~~were~~ compared with analytical predictions and were found to overpredict the induced downwash by 25-35%. ~~The vortex lattice method (VLM)~~ was used to study the effects of: rectangular vs swept wings on induced downwash; tanker tailplane on the receiver; change of angle of attack of one aircraft due to the presence of the other; and the presence of the tanker on the receiver's

pitching moment. Again, the results for induced downwash were compared with the Douglas predictions to evaluate the accuracy. VLM results varied from the Douglas prediction for induced downwash by only 5% and were even more accurate at lower tanker angles of attack. Other findings were: swept wings were necessary for good simulation, the tanker tailplane has only a slight effect on the receiver, and the tanker (in this combination of aircraft) affects the receiver to a greater extent than the receiver affects the tanker. The results indicate that a simple vortex lattice method which ignores fuselage effects, can be used to determine many of the interference effects experienced during aerial refueling.

A Study of the Aerodynamic Interference
Effects During Aerial Refueling

I. Introduction

Background

In April 1923, the first air refueling took place between two Army Air Corps DH-4B aircraft. Since then a variety of aircraft has been used as both tankers and receivers. In the past, refueling training was accomplished in flight. However, with the rising cost of both fuel and airframe time, the Air Force became interested in decreasing the actual flying time while maintaining the same flying proficiency. This was especially true with heavy (B-52, C-141, C-5A) type aircraft. The most logical way to accomplish this task was to develop a simulator that can be used for air refueling training and pilot proficiency requirements.

The Simulator Systems Program Office of Aeronautical Systems Division (ASD) needs a method to provide flow field data for the KC-10 tanker to use in receiver simulator design. This information is necessary to ensure that the receiver simulator "flies" like the real aircraft.

During aerial refueling, the normal position of the receiver aircraft is below and behind the tanker. In the refueling position, the presence of the tanker causes

significant changes in the aerodynamic behavior of the receiver. Therefore, for effective refueling simulation, it is of prime importance to determine how the tanker aerodynamically affects the receiver.

Purpose

The objective of this study was to determine if an analytical or a simple numerical approach can be used for the evaluation of air refueling aerodynamics. To accomplish this, it was necessary to identify the important aerodynamic factors and also determine the complexity of the model required to give acceptable results.

The following effects were considered:

1. Tanker span-wise lift distribution on the flow field.
2. Sweepback of the tanker and the receiver on the flow field.
3. Tanker tailplane on the receiver.
4. Change of the tanker angle of attack due to the receiver.
5. Change of the receiver angle of attack due to the tanker.
6. Change of the receiver's pitching moment due to the tanker.

The fuselage effects of both tanker and receiver aircraft were not considered in the analysis. This greatly simplified the problem and comparison of the computed values with the available Douglas data (5), indicated that it was a reasonable assumption. A discussion of the method used by Douglas, and the effects

they considered, is found in Chapter five.

Approach

The study of the aerodynamic effects of one aircraft on another is not a new problem. In fact, aerial refueling aerodynamics is similar to biplane aerodynamics. In biplane theory, the vertical distance between the two wings is called gap and the horizontal distance between the quarter chords of the two wings is called stagger. The most basic method to model the tanker and receiver is to replace each aircraft with a rectangular wing. The refueling situation is now reduced to a biplane problem with an exaggerated stagger and gap.

Glauert (8), Von Mises (18), Munk (13), Millikan, (12) and others developed biplane theory. They found that, for an elliptical lift distribution on the lead wing, a numerical solution is required to calculate the induced normal velocity at any point in the flow (10). To keep the problem analytical and identify key parameters, three different linear distributions for the tanker wing were selected. They are the tent distribution (Fig 1), the modified linear distribution (Fig 2), and a single horseshoe vortex (Fig 3).

To extend the analytical approach and investigate the effects of sweepback and the tanker tailplane, a vortex lattice method (VLM) was used. In this method, aircraft wings and tailplanes are modeled by flat plate

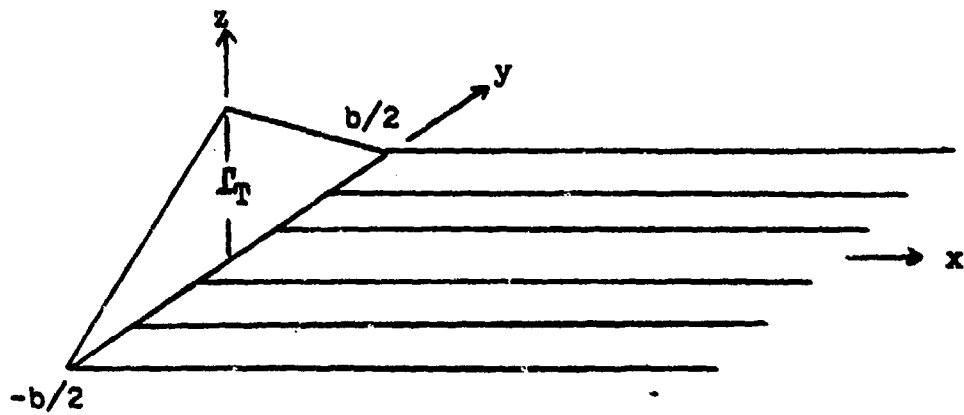


Fig.1. Tent Circulation Distribution

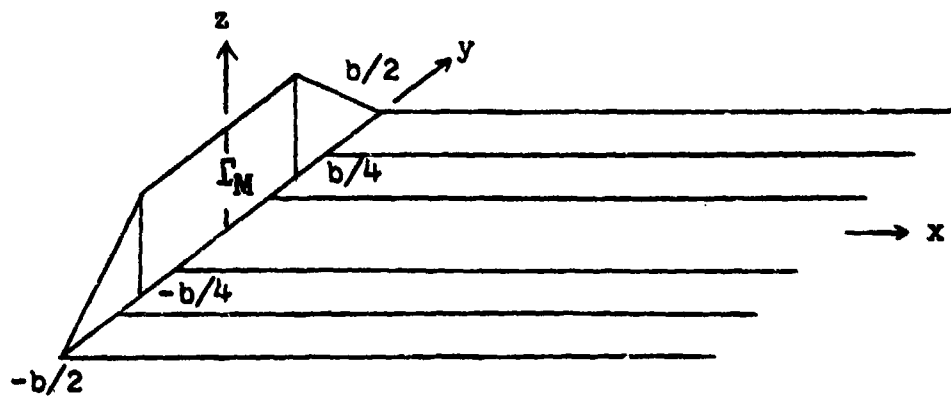


Fig.2. Modified Linear Circulation Distribution

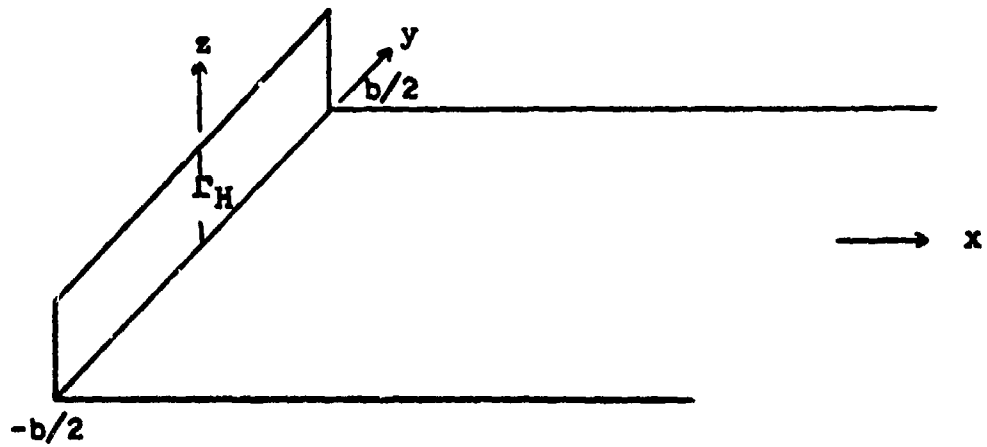


Fig.3. Horseshoe Vortex Circulation Distribution

planforms for a variety of configurations and positions. A KC-10 tanker and a B-52 receiver were used in the evaluation, however, the method can be applied to any tanker and any receiver.

Result Summary

The results of the analytical approach and the vortex lattice method were compared with Douglas Aircraft Company (Douglas) data (5). It was found that the analytical methods were in qualitative agreement for tanker induced velocity, while the vortex lattice results showed excellent agreement with the Douglas data, especially at lower angles of attack, where linear theory is expected to give best results.

II. Air Refueling - A Receiver Pilot's Perspective

To have an accurate simulation, it is necessary to have a thorough knowledge of the process that is simulated. The same is true for the refueling problem. This chapter qualitatively describes the air refueling process from a pilot's point of view. A typical refueling of a KC-135 tanker and a B-52 receiver will be discussed first, followed by a description of the changes caused by refueling with a KC-10 tanker.

A good starting point for the air refueling process is when the B-52 receiver is one mile behind and 1000 feet below the tanker. The B-52 then climbs to a position 1/2 mile behind and 500 feet below the KC-135. The B-52 continues climbing and closing on the tanker to a point slightly behind and below the tanker. This point is called the precontact position (approximately fifty feet behind and ten feet below the contact or refueling position) and is very important. The B-52 is stabilized (closure rate is reduced to zero) at the precontact position. Precontact is important for two reasons:

1. The power setting, trim (angle of attack), and airspeed are approximately the same for the contact position (when the receiver can onload fuel).
2. The aerodynamic effects between aircraft become much more noticeable to the pilots.

As the B-52 moves from precontact to the contact position, the receiver pilot attempts to keep the B-52 on tanker center line, while moving the aircraft forward and slightly up. This is often a difficult task for the refueling student pilot due to the complexity of the combined effects of flying two large aircraft in the same airspace. During the closure to the contact position, the KC-135 must put in nose-up trim to maintain level flight conditions. Approximately seven feet from the contact position, the B-52 experiences a drag increase (may require a slight throttle increase), and a nose up trim requirement. However, after passing that point, there is a slight nose down trim requirement and a drag decrease (may require reduction of throttle setting). While in contact with the tanker, the B-52 can move laterally four degrees (measured from the tanker boom) left or right of tanker centerline with little effect on the B-52 rolling moment (7:1-7). If the B-52 moves laterally more than four degrees, a rolling moment is induced on the B-52, causing it to roll toward tanker centerline.

Refueling with the KC-10 tanker is very similar to the KC-135, with the following exceptions. The KC-10 has a larger wing span than the KC-135 (165 ft vs 131 ft) and also a much heavier gross weight (590,000 lbs vs 297,000 lbs). When a B-52 moves from precontact to contact on the KC-10, there is no increase in drag at the seven foot point as with

the KC-135. Also, the B-52 can move eight to ten degrees left or right of tanker centerline without getting the tendency to roll. Finally, the KC-10 boom is much longer than that of the KC-135 boom and keeps the receiver farther behind and below the KC-10.

A well designed simulator should "fly" the same as the aircraft. Therefore, the previous information will be qualitatively used to check the results. For more information on B-52 refueling procedures, see B-52 T.O.

1-1C-1-15 (7).

III. Analytical Approach

Mathematically modeling the velocity induced on the receiver due to the presence of a tanker was done by three methods. A linear circulation distribution, located at the quarter chord, was assumed for all three methods, so that the equations could be analytically integrated (See Appendix A). Methods 1 and 2 used a lifting line at the quarter chord followed by vortex sheet to represent the tanker. These methods did not simulate roll-up of the vortex sheet. Method 3 used one horseshoe vortex with the lifting line located at the quarter chord and two trailing vortices to represent the tanker. This simulated two fully rolled up tip vortices. The above methods were the extreme cases (no roll-up and fully rolled up vortex sheets) of what actually occurs.

The linear circulation distributions for the tanker in Methods 1, 2, and 3 were selected for two reasons. One, to keep the integration as simple as possible and still give qualitatively useful results. Two, evaluate how a substantial change in lift distribution affected the prediction of induced velocity.

The effect of the rolling up process will be slight. Vortices for a sweptwing aircraft are fully rolled up at three to four span widths (11:13). For a KC-10, that amounts to 660 feet behind the wing tip. In a typical

U
situation, a receiver is only 25 feet behind the tanker.
The descent velocity of the vortex pair was found by (11:8):

$$V_d = \frac{\Gamma_0}{2\pi b'} + \frac{V_d}{4}$$

where b' is the distance separating the two vortices
($b' = \pi b/4$ for an elliptical lift distribution.) For a
typical refueling, $V_d = 5.7 \pm 1.42$ ft/sec.

Notice in Fig 4, the B-52 flight path is well below
the KC-10 tip vortices. Even in the contact position,
the receiver is twenty-five feet below the tanker's wing
tips and the tip vortices are only beginning to roll-up,
indicating that the effect of the rolling-up process should
be minimal. The other assumptions for the analytical
approach are:

1. Linearized potential flow field
2. Receiver is on tanker centerline ($y=0$)
3. Tanker and receiver are represented by
circulation distributions along the
quarter chords (fuselage effects and
tailplanes ignored)
4. Sweepback is not considered

Both tanker and receiver wings induced a downwash at the
receiver wings quarter chord. The total downwash (w_2)
on the receiver wing was found by:

$$w_2 = w_{21} + w_{22}$$

where w_{21} is the induced velocity caused by the tanker on

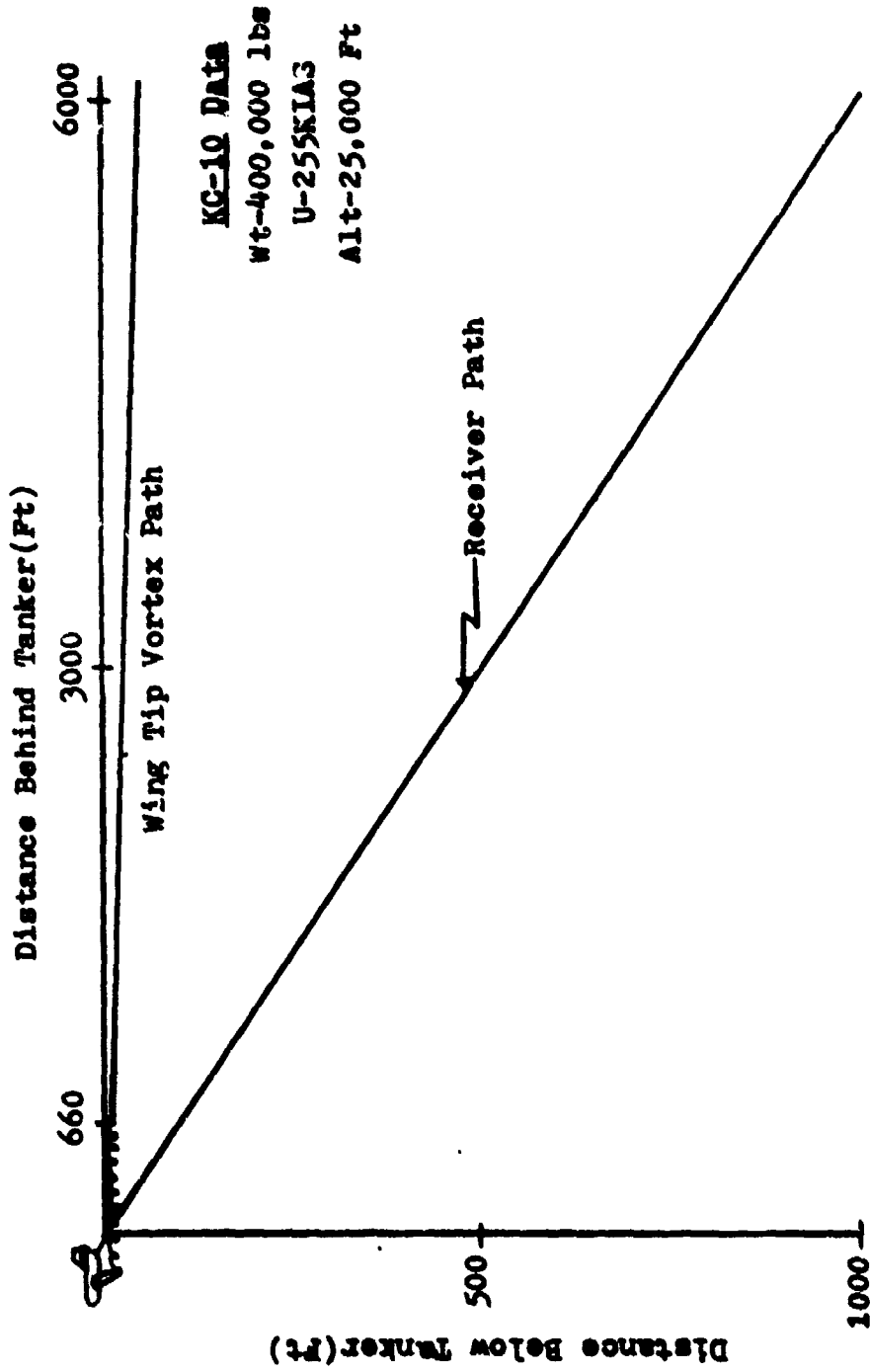


Fig. 4, Receiver Approach Path in Relation to the Location of the Tanker Tip Vortices

the receiver and w_{22} is the velocity the receiver's wing induces on itself.

For all methods discussed above, equations were derived to express the induced velocity at any point in space. To get the tanker influence on the receiver (w_{21}), points were chosen along the lifting line on the receiver's wing.

Method 1

As noted above, method 1 replaces the tanker wing by a lifting line and a semi-infinite vortex sheet combination (Fig 5). Method 1 assumes a tent shaped circulation distribution (Fig 1). An expression for the velocity induced at any point P by the bound vortex (along the y axis) and the planer vortex sheet (in the x, y plane) is derived in Appendix A.

The velocity induced in the x direction (u), is much smaller than the free stream velocity ($u \ll U$) so it is neglected. The velocity induced in the y direction (v) will always average to be zero, provided the receiver is on tanker centerline which was an assumption for the study. Finally, the velocity induced in the z direction (w), is found to have a significant affect on the receiver's flow field.

The induced velocity in the z direction (downwash) is given by Eq (22) in Appendix A. Eq (22) was nondimensionalized by dividing by the free stream velocity (U). Sub-

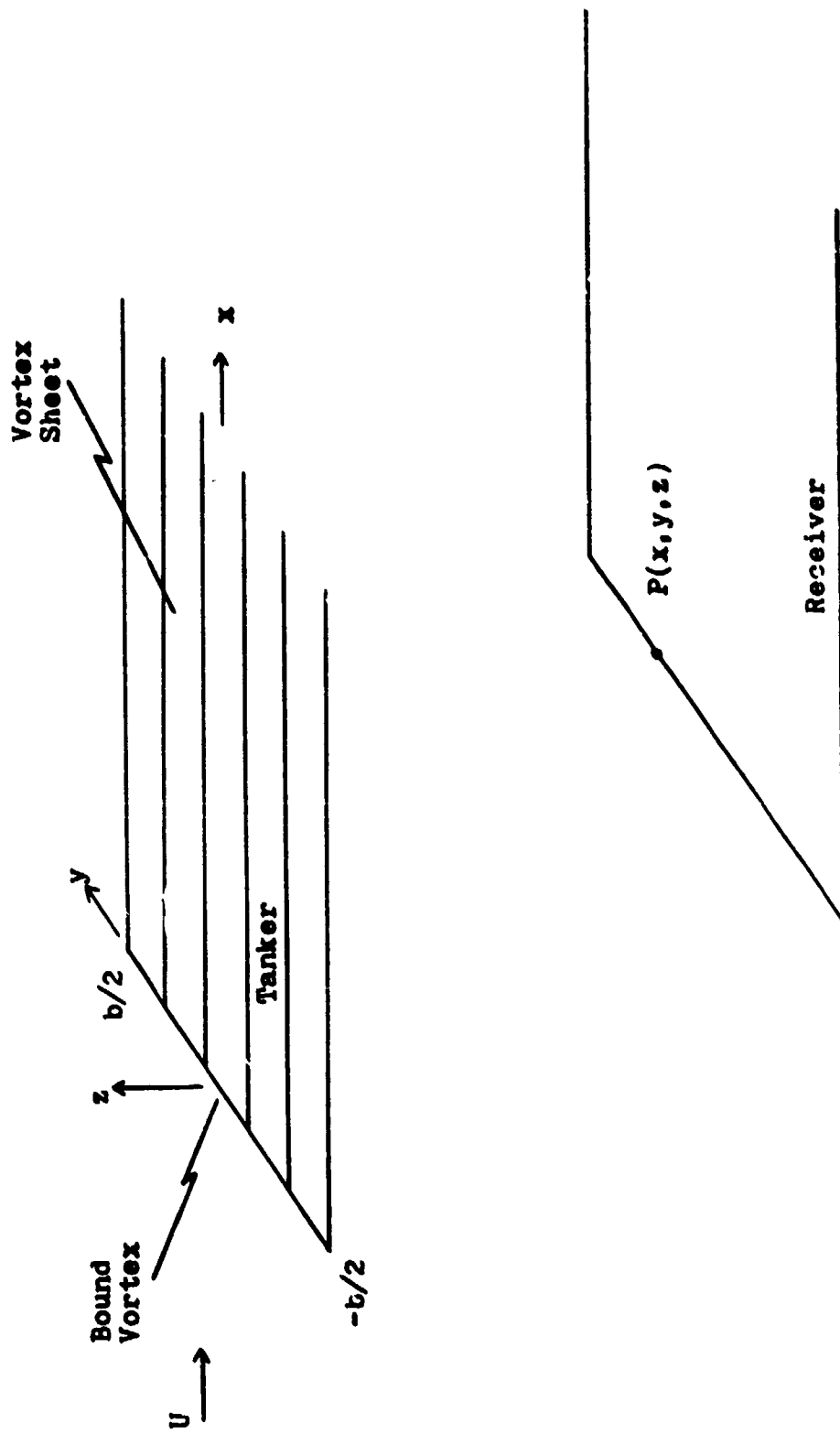


Fig. 5. Sketch of Assumed Tanker wing

stituting Eq (32) for Γ_z yields the induced velocity for any point in space caused by a tent circulation distribution. Thus:

$$\begin{aligned} \frac{w_{21}}{u_\infty} = & \frac{-C_L S}{4\pi b} \left[\frac{x(b/2+2y+2R/b)}{(x^2+s^2)(R+b^2/4+yb)^{3/2}} + \frac{x(b/2-2y+2R/b)}{(x^2+s^2)(R+b^2/4-yb)^{3/2}} \right. \\ & - \frac{x4R}{b(x^2+s^2)R^{3/2}} - \frac{1}{b} \ln \left| \frac{y^2+s^2}{y^2+s^2+by+b^2/4} \right| + \frac{1}{b} \ln \left| \frac{s^2+y^2+b^2/4-by}{s^2+y^2} \right| \\ & - \frac{2}{b} \ln \frac{(R)^{3/2}-x}{R+x} + \frac{1}{b} \ln \frac{(R+yb+b^2/4)^{3/2}-x}{(R+yb+b^2/4)^{3/2}+x} \\ & \left. + \frac{1}{b} \ln \frac{(R-yb+b^2/4)^{3/2}-x}{(R-yb+b^2/4)^{3/2}+x} \right] \quad (2) \end{aligned}$$

In Eq (2) the following information is needed to determine the downwash the tanker induces on the receiver:

1. Tanker lift coefficient (C_L)
2. Tanker reference area (S)
3. Tanker wing span (b)
4. Point of interest P (x,y,s)

Method 2

Similar to method 1, method 2 also models the tanker wing by a lifting line at the quarter chord and a semi-finite vortex sheet combination (Fig 5). Method 2, however, assumes a modified linear shaped circulation distribution (Fig 2). The only difference between Method 1 and Method 2 is the shape of the circulation distribution; therefore, the discussion for Method 1 also applies to Method 2.

From Appendix A, the induced downwash caused by a

modified circulation distribution at any point P(x,y,z) was given by Eq (25). Equation (25) was also nondimensionalized by dividing by the free stream velocity. By substituting Eq (33) for Γ_M , the final result for the modified circulation distribution is:

$$\frac{w_{21}}{u_\infty} = \frac{-C_L S}{6\pi b} \left[\frac{-x(b/4+2y+4R/b)}{(x^2+z^2)(b^2/16+yb/2+R)^{\frac{1}{2}}} + \frac{x(b+4b+4R/b)}{(x^2+z^2)(R+b^2/4+yb)^{\frac{1}{2}}} \right. \\ - \frac{x(2y-b/4+4R/b)}{(x^2+z^2)(R-yb/2+b^2/16)^{\frac{1}{2}}} + \frac{x(b-4y+4R/b)}{(x^2+z^2)(b^2/4-yb+R)^{\frac{1}{2}}} \\ - \frac{2}{b} \ln \left| \frac{y^2+z^2+b^2/16+yb/2}{y^2+z^2+b^2/4+yb} \right| + \frac{2}{b} \ln \left| \frac{y^2+z^2+b^2/4-yb}{y^2+z^2+b^2/16-yb/2} \right| \\ - \frac{2}{b} \ln \left| \frac{(R+yb/2+b^2/16)^{\frac{1}{2}} - x}{(R+yb/2+b^2/16)^{\frac{1}{2}} + x} \right| + \frac{2}{b} \ln \left| \frac{(R+yb+b^2/4)^{\frac{1}{2}} - x}{(R+yb+b^2/4)^{\frac{1}{2}} + x} \right| \\ \left. + \frac{2}{b} \ln \left| \frac{(R-yb+b^2/4)^{\frac{1}{2}} - x}{(R-yb+b^2/4)^{\frac{1}{2}} + x} \right| - \frac{2}{b} \ln \left| \frac{(R-yb/2+b^2/16)^{\frac{1}{2}} - x}{(R-yb/2+b^2/16)^{\frac{1}{2}} + x} \right| \right] \quad (3)$$

The information needed to determine the downwash the tanker induces on the receiver in Eq (2) also applies to Eq (3).

Method 3

The previous results are for a vortex sheet with a linear circulation distribution, simulating no vortex roll up. To try to bracket the problem, a single horseshoe vortex, simulating fully rolled up tip vortices, may be used to represent the tanker wing. The derivation for the velocity induced by any horseshoe vortex is found in (1:191-201). Figure 6 shows the tanker wing represented by a horseshoe vortex.

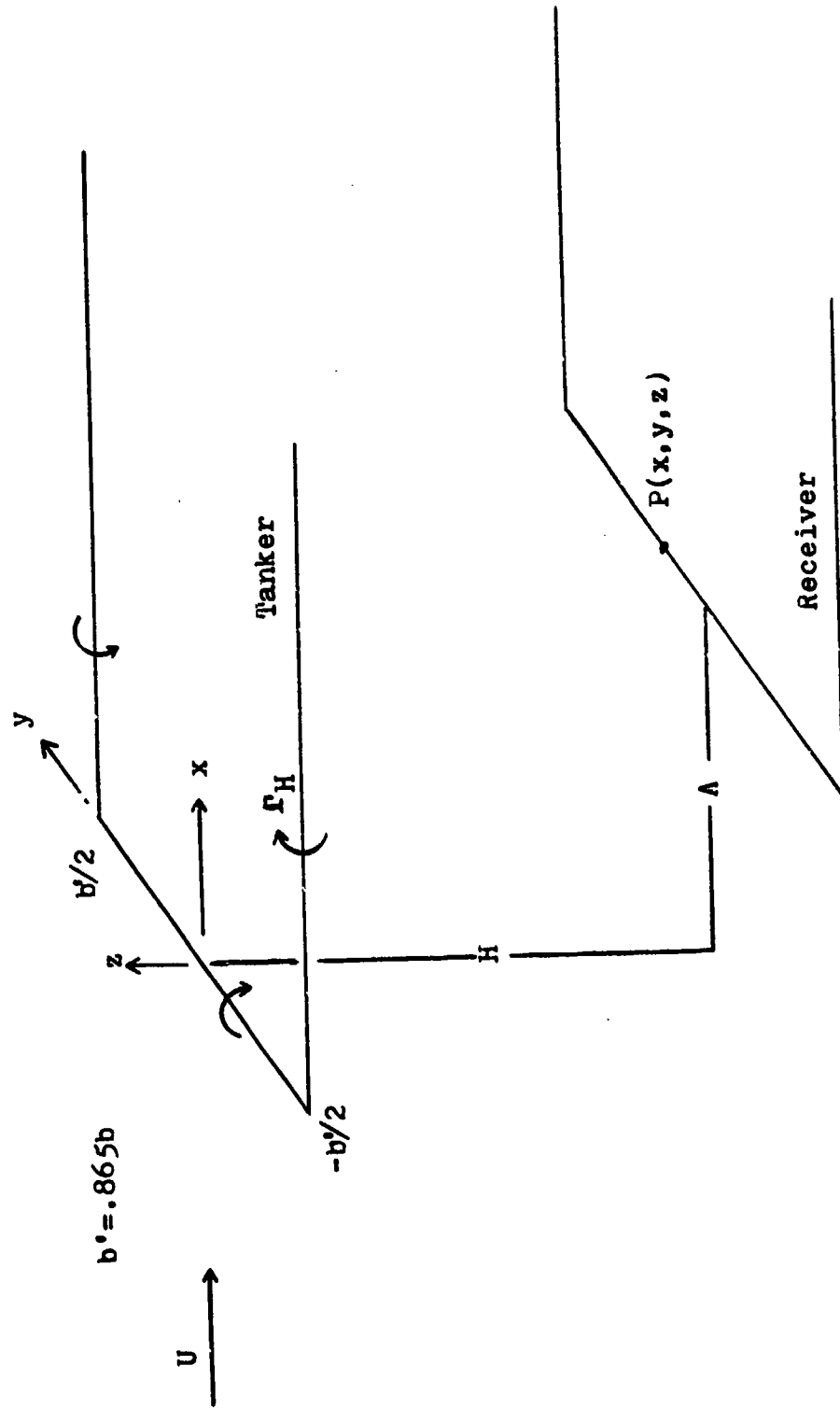


Fig.6. Sketch of a Horseshoe Vortex Modeling the Tanker

Again, select point P on the lifting line of the receiver to get the downwash of the tanker on the receiver. Then vary P along the lifting line to compute the downwash distribution.

A modified tip wing span b' represents the effective wing span due to the roll up of the tip vortices.

Muttray (14) states the correction for the span with a constant lift distribution is .865, therefore $b' = .865b$ was used.

From the 3D horseshoe vortex derivation in (1:197), the induced downwash at any point in space is:

$$w_{21} =$$

$$\frac{\Gamma_H}{4\pi} \left(\frac{(x-x_1)(y-y_2) - (y-y_1)(x-x_2)}{\{(y-y_1)(z-z_2) - (z-z_1)(y-y_2)\}^2 + \{(x-x_1)(z-z_2) - (z-z_1)(x-x_2)\}^2} \dots \right. \\ \left. \dots \frac{1}{\{(x-x_1)(y-y_2) - (y-y_1)(x-x_2)\}^2} \right)$$

$$\left[\frac{(x_2-x_1)(x-x_1) + (y_2-y_1)(y-y_1) + (z_2-z_1)(z-z_1)}{\{(x-x_1)^2 + (y-y_1)^2 + (z-z_1)^2\}^{\frac{1}{2}}} \right. \\ \left. \frac{-(x_2-x_1)(x-x_2) + (y_2-y_1)(y-y_2) + (z_2-z_1)(z-z_2)}{\{(x-x_2)^2 + (y-y_2)^2 + (z-z_2)^2\}^{\frac{1}{2}}} \right]$$

$$\begin{aligned}
 & + \frac{y_1 - y}{(z - z_1)^2 + (y - y_1)^2} \left[1 + \frac{x - x_1}{(x - x_1)^2 + (y - y_1)^2 + (z - z_1)^2} \right] \\
 & - \frac{(y_2 - y)}{(z - z_2)^2 + (y - y_2)^2} \left[1 + \frac{x - x_2}{(x - x_2)^2 + (y - y_2)^2 + (z - z_2)^2} \right]
 \end{aligned}$$

where x, y, z are the coordinates of point P.

As indicated in Fig 6,

$$x_1 = x_2 = 0$$

$$z_1 = z_2 = 0$$

$$x = A$$

$$z = H$$

$$y_1 = -.865b/2$$

$$y_2 = .865b/2$$

Substituting these values into Eq (4) yields:

$$\begin{aligned}
 w_{21} = \frac{\Gamma H}{4\pi} & \left(\frac{1.156A}{bA^2 + H^2b} \left[\frac{.865b(y + .4325b)}{(.187b^2 + .865yb + R)^{\frac{1}{2}}} - \frac{.865b(y - .4325b)}{(.187b^2 - .865yb + R^2)^{\frac{1}{2}}} \right] \right. \\
 & + \frac{(-.4325b - y)}{H^2 + (y + .4325b)^2} \left[1 + \frac{A}{(.1876b^2 + .865yb + R)^{\frac{1}{2}}} \right] \\
 & \left. - \frac{(.4325 - y)}{H^2 + (y - .4325b)^2} \left[1 + \frac{A}{(.187b^2 - .865yb + R)^{\frac{1}{2}}} \right] \right) \quad (5)
 \end{aligned}$$

The circulation is found from: $\Gamma_H = \frac{L}{\rho u_{\infty} b}$ (See Appendix B for derivation.)

Dividing Eq (5) by U yields a nondimensional equation for downwash. Thus, Eq (5) becomes:

$$\frac{w_{21}}{U} = \frac{C_L S}{8\pi b} \left\{ \frac{1.156A}{bA^2 + bH^2} \left[\frac{.865b(y + .4325b)}{(.187b^2 + .865yb + R)^{\frac{3}{2}}} - \frac{.865b(y - .4325b)}{(.187b^2 - .865yb + R)^{\frac{3}{2}}} \right] + \frac{(-.4325b - y)}{H^2 + (y + .4325b)^2} \right. \\ \left. \left[1 + \frac{A}{(.187b^2 + .865yb + R)^{\frac{3}{2}}} \right] - \frac{(.4325 - y)}{H^2 + (y - .4325b)^2} \right\} \quad (6)$$

In Eqs (2), (3), and (6), downwash information for the receiver flowfield is determined by varying P (x,y,z) along the receiver's lifting line.

Once the downwash velocity the tanker induces on the receiver is calculated, the relative velocity for the receiver can be determined. This relative velocity is found by the vector addition of the free stream velocity and the tanker induced downwash velocity. The aerodynamic coefficients are calculated using both the relative and free stream velocities, and the differences between the coefficients are the aerodynamic interference effects.

In the above equations, changing the tanker gross weight is accomplished by varying the tanker coefficient of lift. Finally, any tanker can be modeled by changing

the values of wingspan and wing area.

Compressibility Considerations

The compressibility effects on downwash were taken into account by the Goethert transformation (2). The parameters were transferred as follows:

<u>Incompressible</u>	<u>Compressible</u>
C_L	BC_L
x	x/B
y	y
z	z
b	b

where $B = (1 + M_\infty^2)^{\frac{1}{2}}$

A discussion of the results obtained using Eqs (2), (3), and (6) and comparison with other data, are presented in Chapter Five.

IV. Vortex Lattice Method

To treat more complicated configurations (sweepback, tailplane effects, etc.) a numerical approach is required. The vortex lattice method (VLM) was the numerical technique selected for study because of its well established and proven ability to yield accurate results for interfering lifting surfaces (15:89).

In Chapter three, a single horseshoe vortex was used to represent the tanker's wing. In contrast, the VLM uses multiple horseshoe type vortices to represent a wing. The wing is overlaid by a geometric network of lattice boxes or panels. A typical panel contains a bound vortex and two trailing vortices. The bound vortex is located on the panel's quarter chord. A panel control point is at the center of the three quarter chord of the panel. It is at the control point that the flow tangency boundary condition is enforced. See Fig 7 for a typically panelled wing.

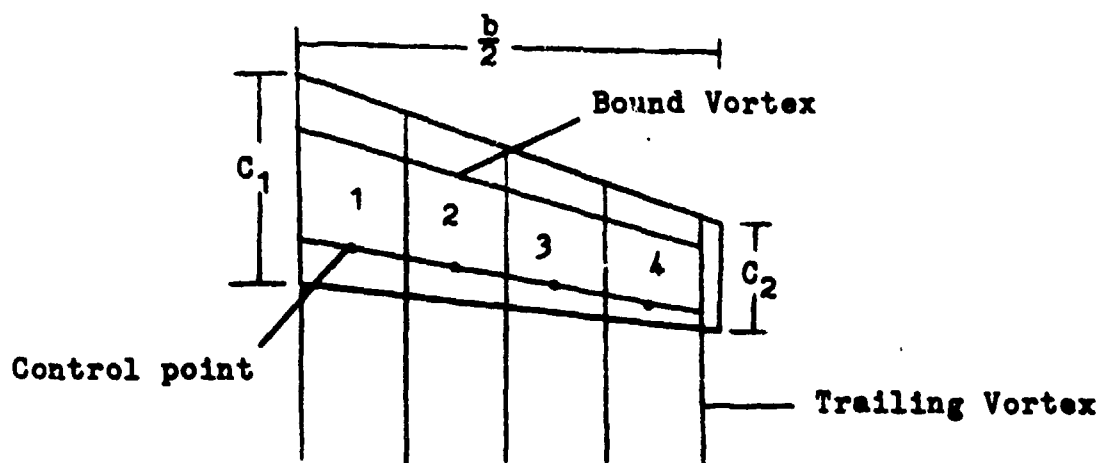


Fig. 7. Vortex Lattice Panelled Wing

Four panels were used to represent the above wing. More accuracy and chordwise resolution of aerodynamic forces can be achieved by using chordwise as well as spanwise panels. To account for tip effects, the last panel was slightly indented from the wing tip. The equation used to determine this distance is (15):

$$y_{\text{tip}} = \frac{b/2}{1 + 1/N_S} \quad (7)$$

where N_S is the number of semispan panels; in the above example, N_S is 4. The slight indentation allows the use of less panels to achieve the same accuracy (15).

Each vortex panel induces a velocity on itself and on all the other panels. This is represented by an influence coefficient matrix A where:

$$\{A\}\bar{\Gamma}_j = \bar{c}_j \quad (7a)$$

A typical element of $\{A\}$, A_{ij} represents the downwash velocity at the control point of panel i induced by a horseshoe vortex at panel j . $\bar{\Gamma}_j$ is the circulation at panel j and \bar{c}_j is the flow tangency boundary condition at panel j . For a planar wing with no dihedral, the flow tangency condition is $\bar{c} = -u_\infty$. Gamma (the circulation vector) is then found by:

$$\bar{\Gamma} = \{A\}^{-1} \bar{c} \quad (8)$$

Once Gamma is known, the aerodynamic force distribution can be determined (See Appendix D). Reference (1) provides more detailed description of the vortex lattice method.

The following assumptions were made in the vortex lattice approach:

1. Linear potential flow
2. Wings are represented by flat plates (no camber or twist)
3. Fuselage effects are ignored
4. Wing tip vortex roll up is ignored
5. Receiver is on tanker centerline ($y_{C_L} = 0$)

An existing computer program called LATEX (Appendix C) was selected for evaluation. LATEX uses the vortex lattice method. The significant advantages of LATEX are its simplicity, ability to handle more than four lifting surfaces, and direct printout of induced normal velocity.

The coordinate system was set up such that the z direction is perpendicular to the tanker wing at zero angle of attack (positive up), x is in the downstream direction, and y makes an orthogonal system going out in the direction of the tankers right wing. The coordinate system is independent of the angle of attack, therefore, to use the coefficient in the normal direction (C_z) as the lift coefficient, the small angle assumption is made. The origin used is always at the tanker wing's leading edge centerline (See Fig 8).

Two methods may be used to change angle of attack in

C

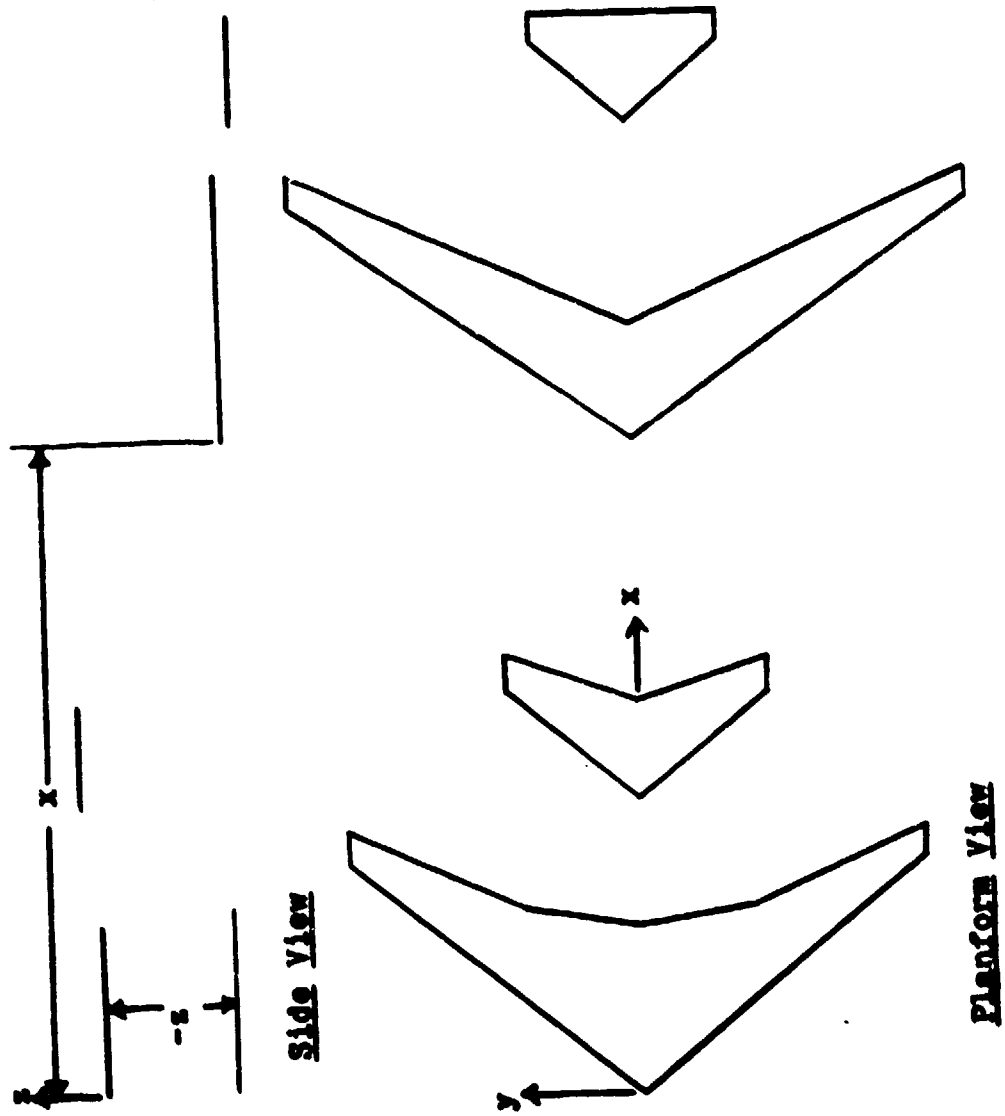


FIG. 8. Refueling Coordinate System

the LATEX Program. A geometric angle of attack generated a constant α (in degrees) for the entire system of lifting surfaces. A second method specifies angle of attack (in radians), by means of a table. The table is part of the input file and is used to change a control point boundary condition (See Appendix C). The advantage of using the input or twist table is that each wing can now be given a different angle of attack. Comparisons using both the geometric α and the input table were made and the results indicated, as expected, that either method provides the same results for the small angles considered.

The wake was modeled to extend in the x (downstream) direction. In the case of the KC-10 wing, the wake extends at $x = 0$ at a constant rate equal to U . The wake does not roll up or descend as an actual wake would do.

The majority of testing was done with four lifting surfaces. These are the KC-10 wing and tailplane, and the B-52 wing and tailplane (See Fig 8). Ten semispan panels were used for the KC-10 wing, twenty semispan panels were used for the B-52 wing, and five semispan panels were used for both tailplanes. LATEX reflects an image of each wing for calculation purposes, so input of only the semi-span data is necessary.

Presently, LATEX has no direct method to determine off body information. It was discovered that panels with large aspect ratio (0.5 ft width by 10 ft length) induced an insignificant amount of downwash on themselves regard-

less of panel angle of attack. When these panels were used for off body information, the induced downwash at these panels was due to the induced velocity of the flow field. Therefore, this type of panel was used for all off body data.

The pitching moment coefficient (C_M) was determined by establishing the B-52 at a desired angle of attack and iteratively selecting a tailplane angle of attack to make $C_M = 0$. The wing angle of attack selected was $\alpha = 6.0^\circ$, which put the B-52 at a typical refueling gross weight. The B-52 center of gravity was selected to be at the quarter mean aerodynamic chord because most refueling is accomplished with the CG near the quarter chord position. The B-52 was then put behind the KC-10 at multiple locations. The B-52 lift was kept constant by iteratively changing its angle of attack at each position behind the tanker. ΔC_M was determined by comparing the C_M for the B-52 alone with the C_M for the B-52 behind the tanker. The results of the Vortex Lattice analysis are found in Chapter Five, and a description on the use of LATEX is found in Appendix C.

V. Results

The results of the analytical approach and the LATEX computer program are compared with Douglas KC-10 data found in (5). These data were generated by a Weissinger Computer Method.

The Weissinger method replaces the wing by a plate of zero thickness that has the planform and twist identical to the wing. The chordwise loading distribution is assumed to be concentrated into a lifting line located at the quarter-chord of the wing. Chordwise control points are chosen to be at the three-quarter-chord line and the flow tangency boundary condition is applied at these points (no flow is allowed through the plate at these points). The lifting line and its trailing vortex sheet are treated to be continuous. Substituting the vortex pattern for the wing and applying the boundary conditions allows the formation of a set of simultaneous equations, which can then be solved. For a more detailed analysis of the Weissinger method, see NACA Report No. 921 by DeYoung and Harper (3).

Tanker lift distribution, tailplane effects, fuselage effects, and depression of the vortex sheet were considered by Douglas in generating the downwash data. No wind tunnel data or flight test data were available for comparison. The analytical results will first be discussed followed by the vortex lattice results.

Analytical Results

Equations (2), (3), and (6) were programmed into an HP-35CV hand calculator. The calculator took approximately 6 seconds to compute a value of downwash at each point. Recall that the analytical solutions represent the entire tanker by a rectangular wing with a linear circulation distribution. Downwash vs span-wise location on the receiver wing is plotted on Figs 9-12.

Figures 9-11 are for the contact position (25 ft below, 125 ft behind the tanker leading edge.) Notice on Fig 9, the tent distribution over-predicts (in comparison with the Douglas data) the induced downwash by 55% at a span position of 0. The modified linear and the horseshoe vortex models (with $b' = .865$ in the latter model) agree on the average within 25-35% of the Douglas data. In Fig 12 the downwash is shown for the precontact position (35 ft below, 175 ft behind the tanker). The analytical curves are closer to the Douglas curve at a distance farther behind and below the tanker, indicating that a more accurate model is needed for close proximity effects, including fuselage, sweepback and tanker tailplane influence.

From Figs 9-11, it can be seen that the analytical equations overestimate the average downwash over a 90 ft semi-span. The modified linear distribution gives a 25% disagreement followed by the horseshoe vortex with a 35% disagreement. It is evident from these figures that the

KC-10 Data
 Weight 590,000lbs
 M=0.6
 $S_{ref}=3647(Ft)^2$

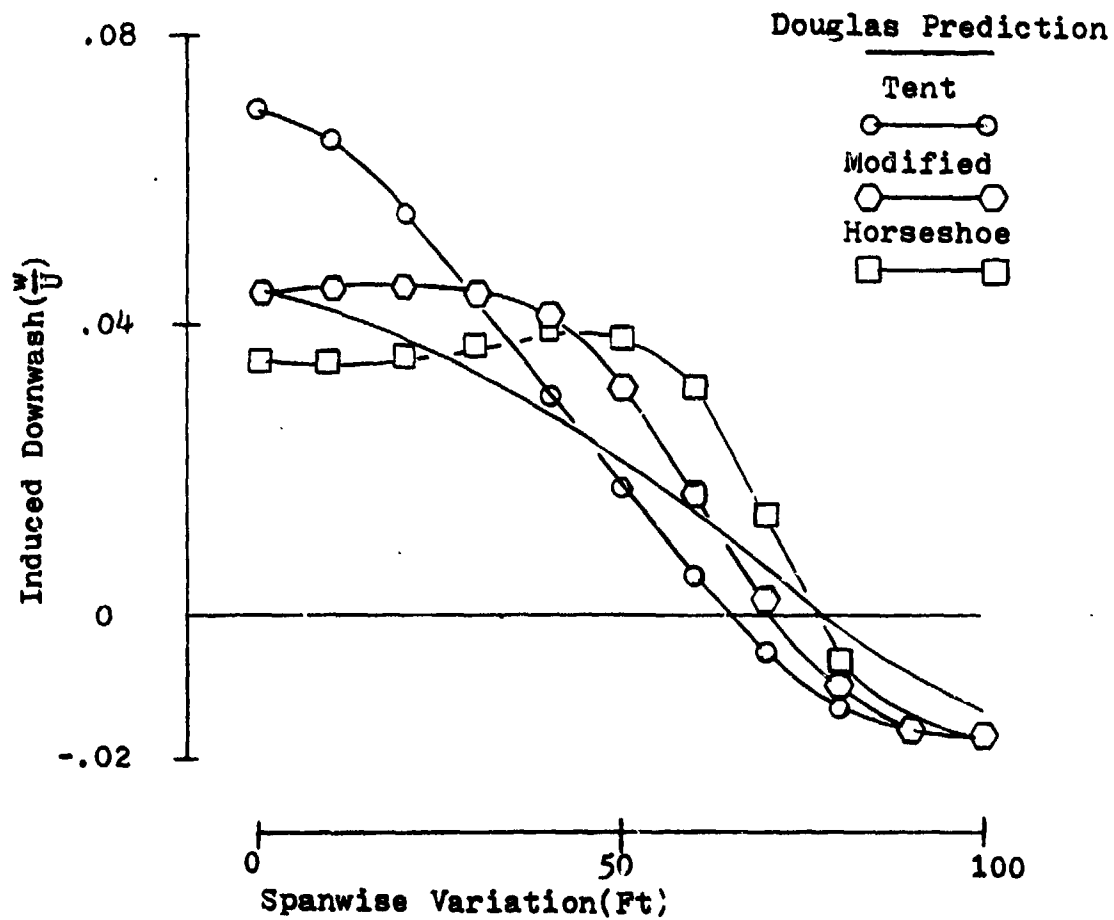


Fig.9. Analytical Downwash vs Span Location
 (Contact Position) Wt=590,000 lbs

KC-10 Data
 Weight 260,000
 M=0.6
 S_{ref}=3647Ft²

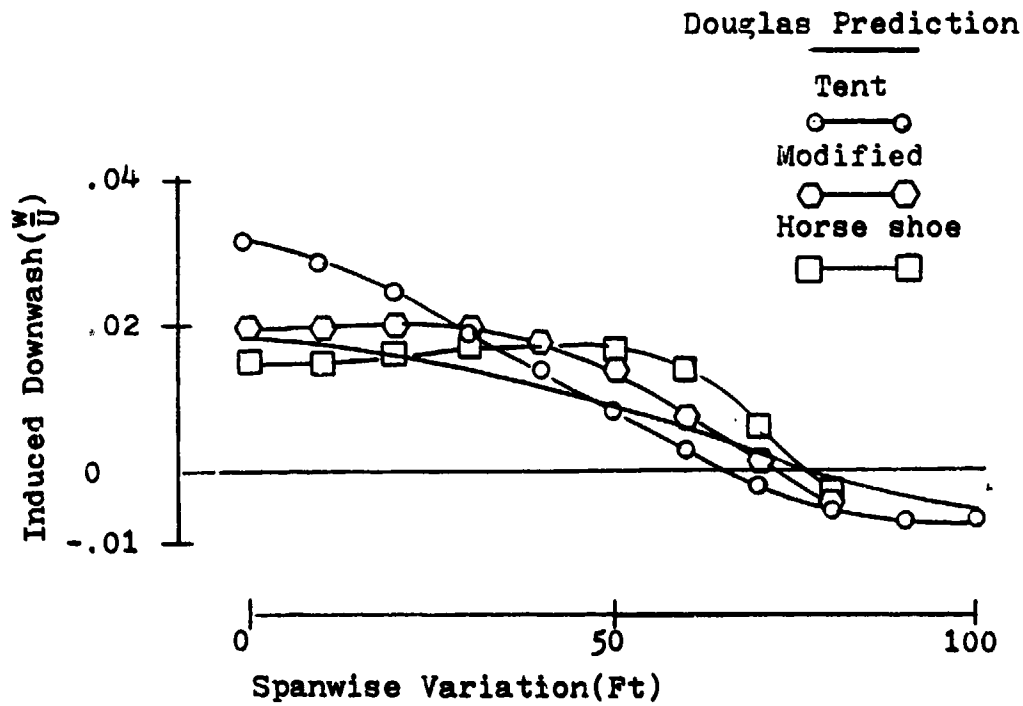


Fig.10. Analytical Downwash vs Span Location.
 (Contact Position) Wt=260,000 lbs

KC-10 Data
 Wt 260,000 lbs
 M=0.36
 Alt 10,000 Ft

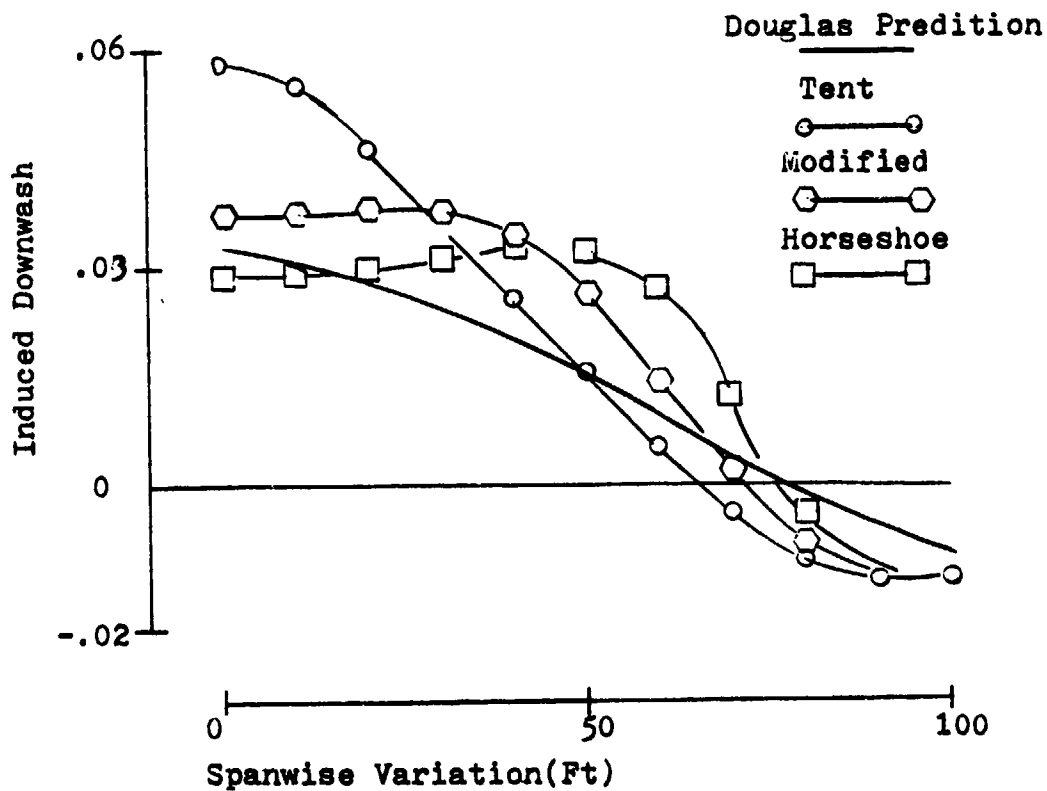


Fig.11. Analytical Downwash vs Span Location
 (Contact Position)

KC-10 Data
 Wt 260,000 lbs
 M=0.36
 Alt =10,000 Ft

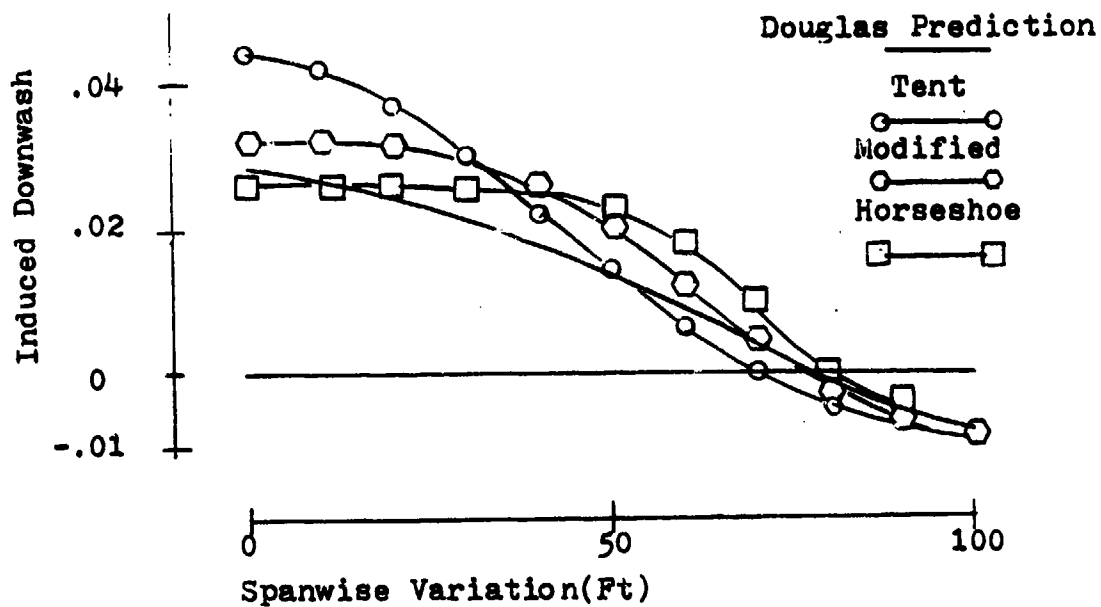


Fig.12. Analytical Downwash vs Span Location
 (Precontact Position)

shape of the tanker lift distribution and sweepback have a substantial effect on the induced downwash.

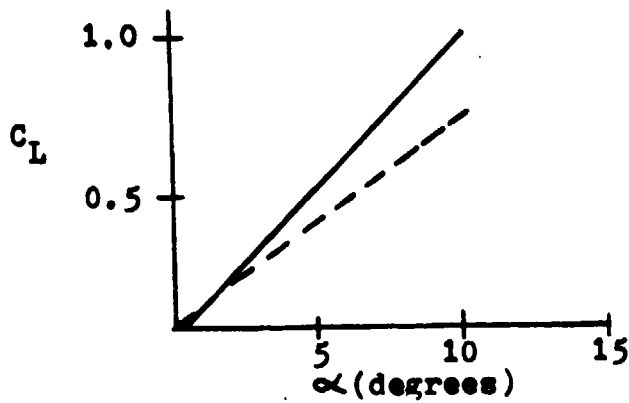
While the analytical equations give a qualitative idea of the tanker flowfield, better results can be achieved using a more sophisticated model. The vortex lattice method not only yields better results, it can also evaluate all of the desired interference effects.

VLM Results

The vortex lattice method was used to study the effects of wing sweep, tailplane influence, change of bomber pitching moment, and how the presence of one aircraft affects the lift of the other aircraft.

The C_L vs α curves are shown for both the KC-10 and the B-52 in Figs 13 and 14. Both flight test derived C_L vs α curves are greater than the curves generated by the vortex lattice method. This is to be expected since the aircraft wings are represented by flat plates in LATEX (i.e., no camber or twist) where in reality, both wings have camber and twist.

Fig 15 shows the effect on induced downwash caused by using a rectangular wing (with the same span and wing area) and the actual swept wing. Results are plotted for the contact and the precontact position. Notice how the swept wing induces more downwash closer to centerline and less downwash farther away from the centerline than the rectangular wing. The figure indicates there is a sig-



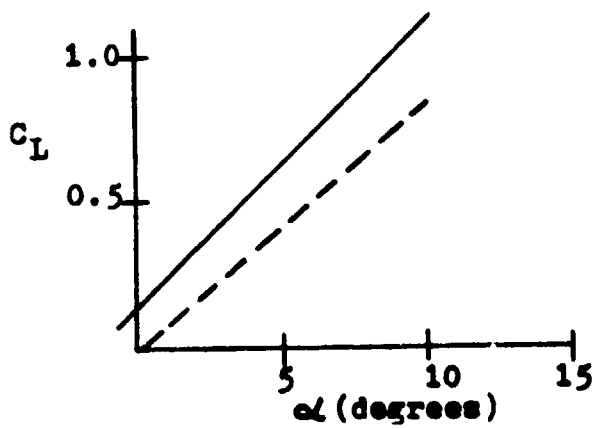
Boeing Data

Vortex Lattice

$S_{ref} = 4000 \text{ Ft}^2$

$M = 0.6$

Fig. 13. B-52 C_L vs α



Douglas Data

Vortex Lattice

$S_{ref} = 3647 \text{ Ft}^2$

$M = 0.6$

Fig. 14. KC-10 C_L vs α

KC-10 Data

$\alpha = 4.5^\circ$

$M = 0.6$

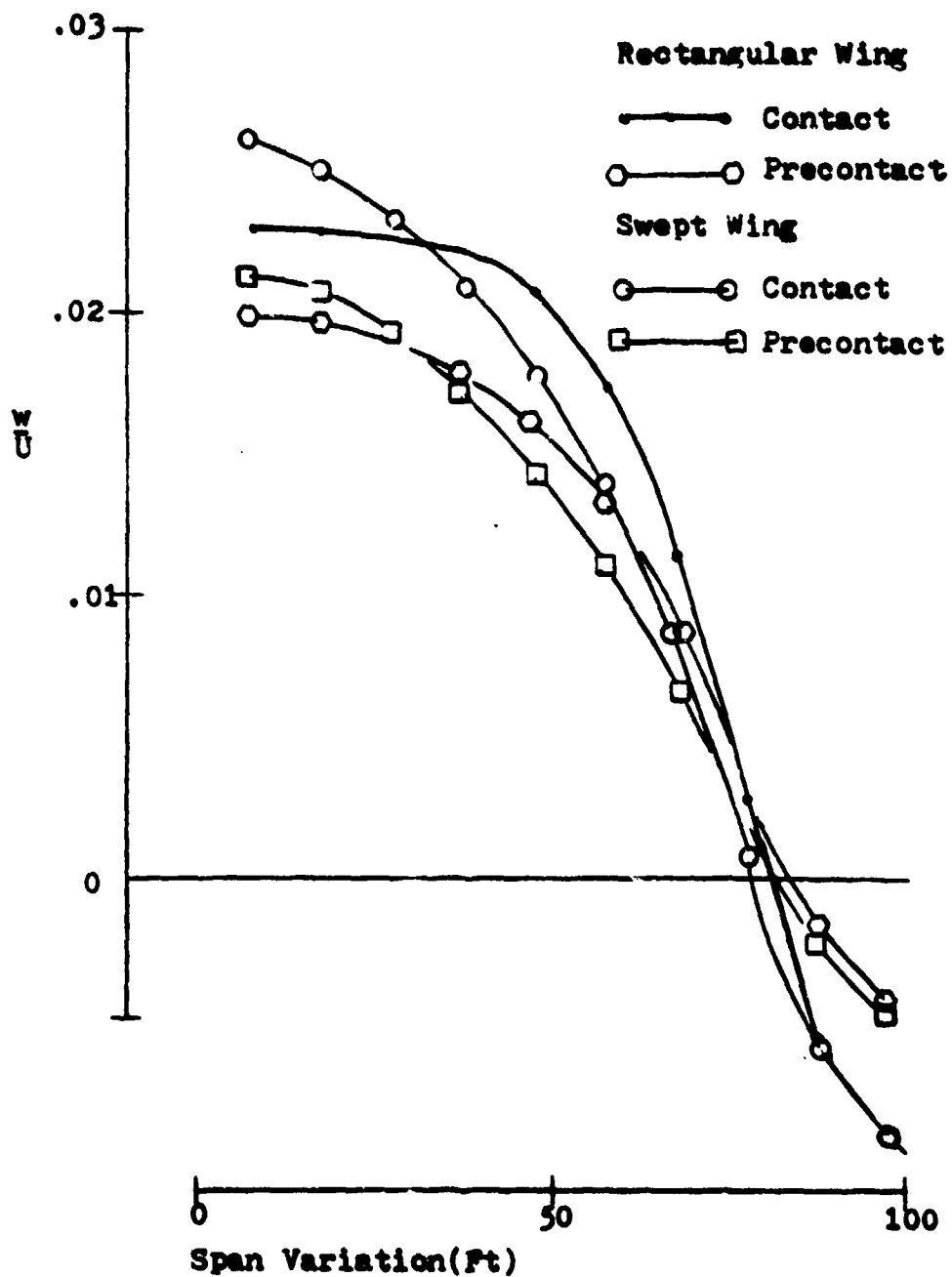


Fig. 15. VLM Downwash Comparison (at the B-52 wing) of Rectangular and Swept Tanker Wings

nificant difference between the swept and rectangular results; therefore, for all computer generated downwash, the actual swept wing planforms will be used for greater accuracy.

Sectional lift coefficient (C_L) vs span for the KC-10 wing is found on Fig 16. The wing was panelled with one chordwise panel and ten semispan panels. Fifty panels and 100 panels per semispan were also evaluated. It was found that when one chordwise panel and ten semispan panels represented the tanker wing, an increased number of panels gave no significant improvement (less than 1% change in induced downwash).

The downwash field behind the KC-10 was evaluated with and without the tanker tailplane. Figures 17-20 indicate the induced downwash vs span from $\frac{1}{2}$ mile to the contact position.

Notice there is only a slight increase in induced downwash, caused by the tanker, as the receiver moves up toward the precontact position. At the contact and precontact positions, the results are compared with the Douglas data. Figures 19 and 20 indicate that the induced downwash is slightly in error with or without the tailplane when the KC-10 angle of attack is 6.8 degrees. However, Fig 21 indicates that the KC-10 with the tailplane matches the Douglas data for an angle of attack of 2.3 degrees. Therefore, inclusion of the tanker tailplane results in more accurate values of

KC-10 Data

$\alpha=6.1^\circ$

$M=0.6$

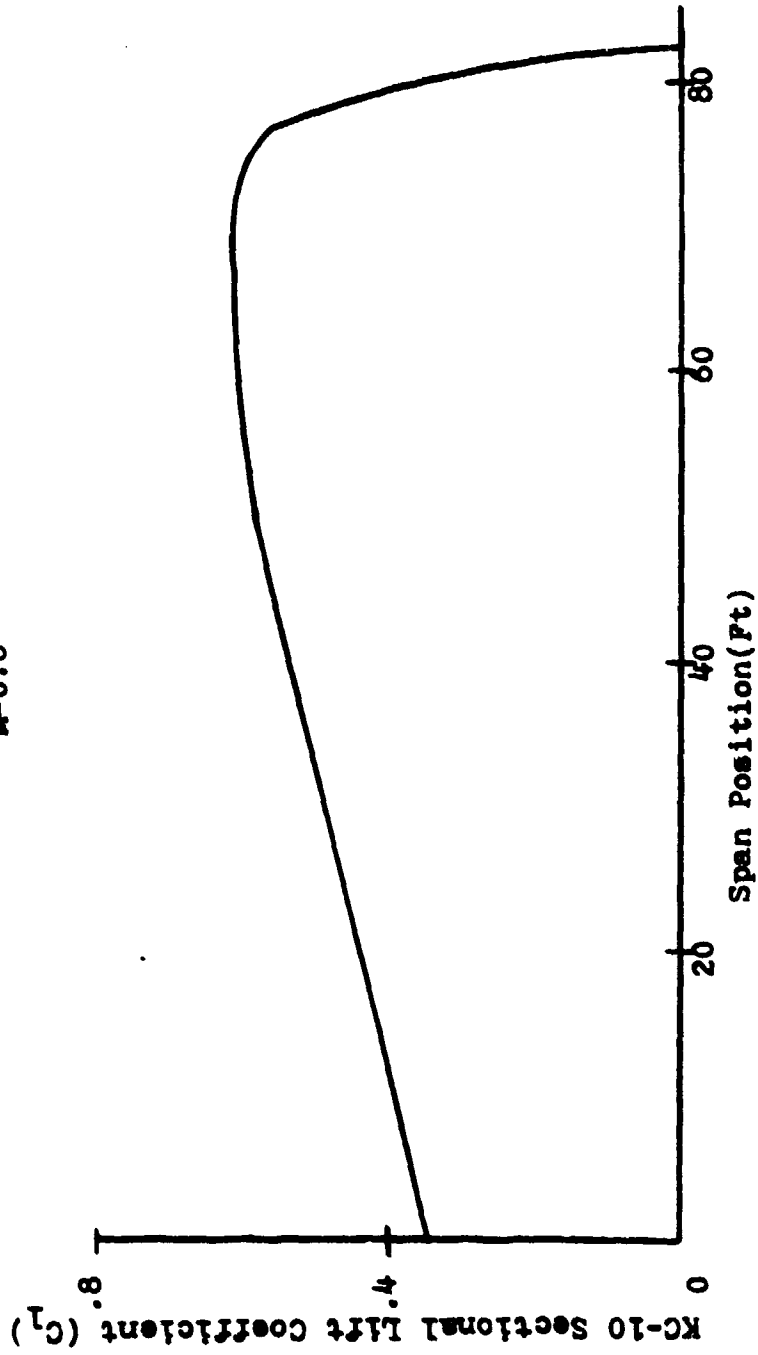


Fig.16. KC-10 Sectional Lift Coefficient vs Span (VLM)

KC-10 Data

$\alpha=6.8^\circ$

$M=0.6$

Position Information

$x=3125$ Ft

$z=-500$ Ft



KC-10 Data

$\alpha=6.8^\circ$

$M=0.6$

Position Information

$x=1650$ Ft

$z=-250$ Ft

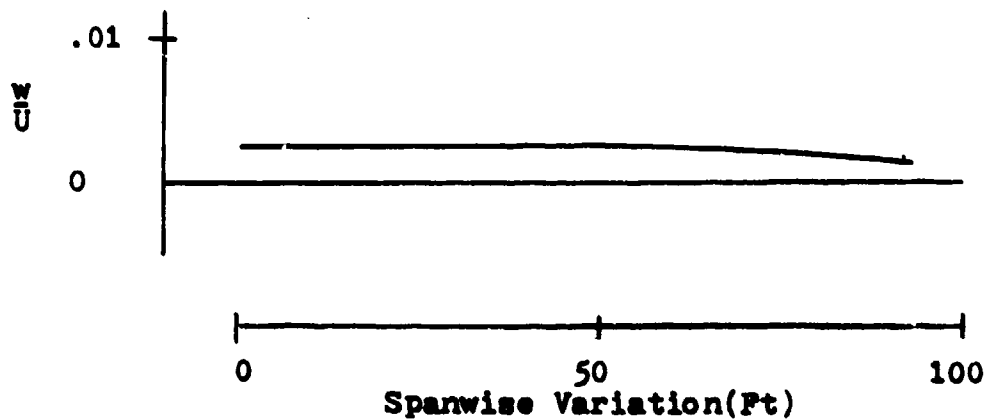


Fig. 17. VLM Induced Downwash vs Span Position

KC-10 Data

$\alpha = 6.8^\circ$

$M = 0.6$

Position Information

$x = 525 \text{ Ft}$

$z = -75 \text{ Ft}$

Tanker Wing And Tailplane

Tanker Wing Alone

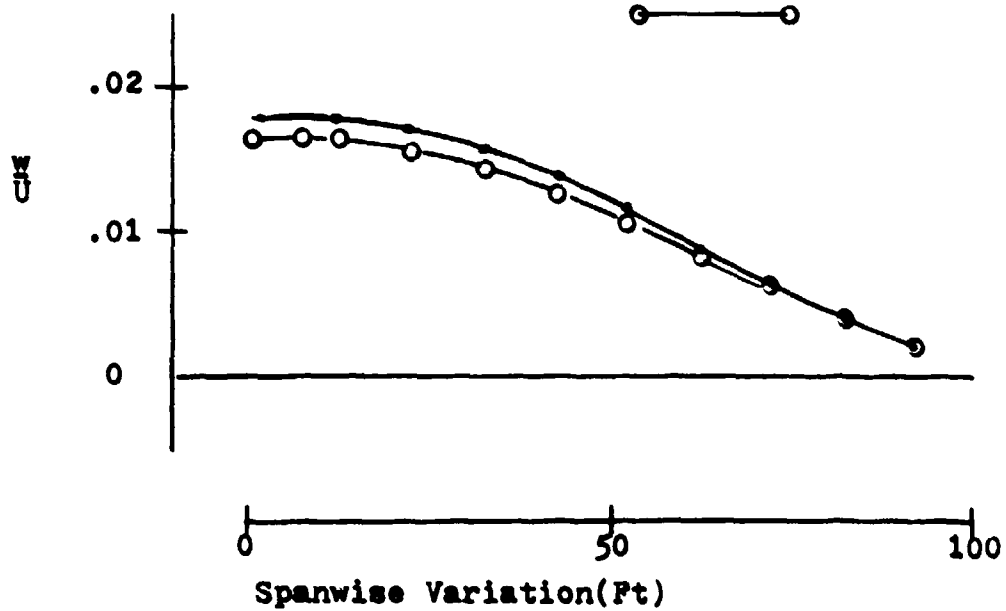


Fig. 18. VLM Induced Downwash vs Span Position

KC-10 Data

$\alpha = 6.8^\circ$
 $M = .6$

Position Information

$x = 175$ Ft (Precontact)
 $z = -35$ Ft

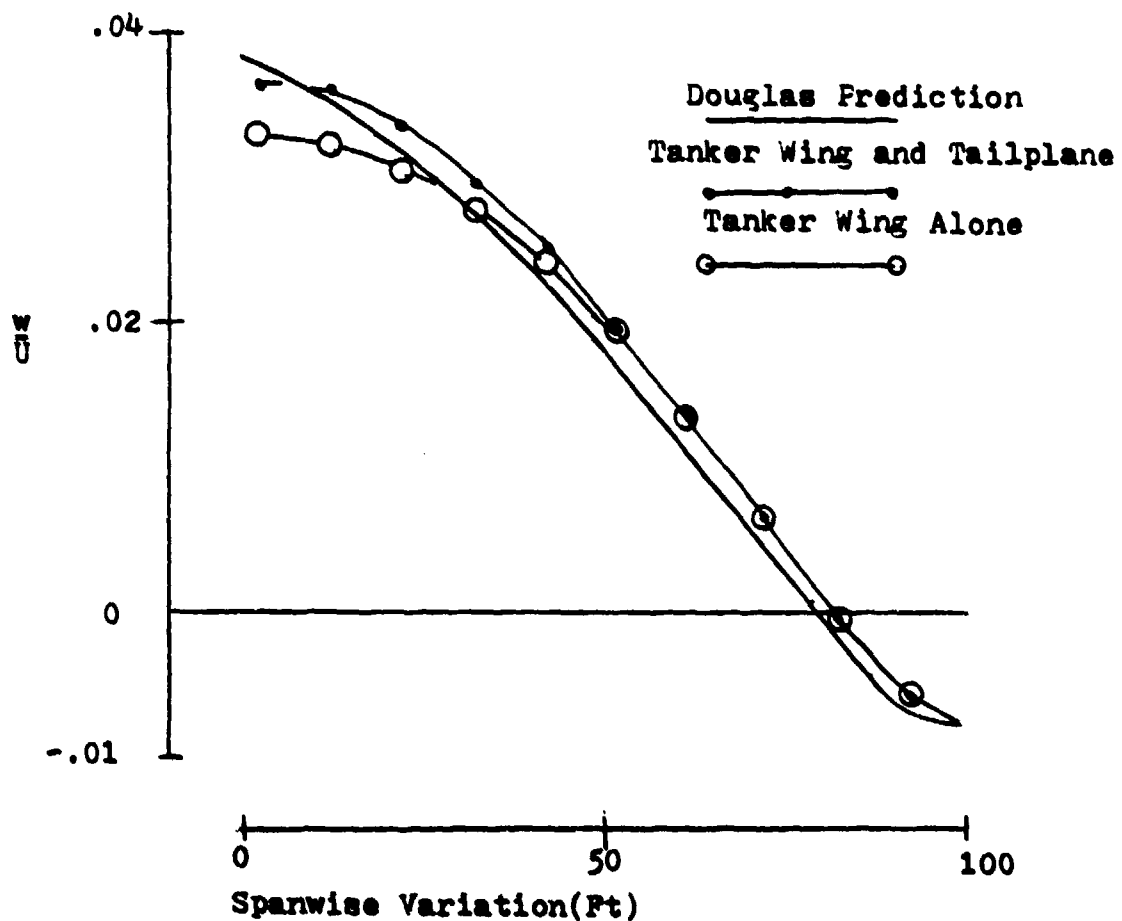


Fig. 19. Induced Downwash vs Span Position(Precontact)

KC-10 Data
 $\alpha = 6.8^\circ$
 Tailplane $\alpha = 4.8^\circ$
 $M = 0.6$

Position Information
 $x = 125$ Ft (Contact)
 $z = -25$ Ft

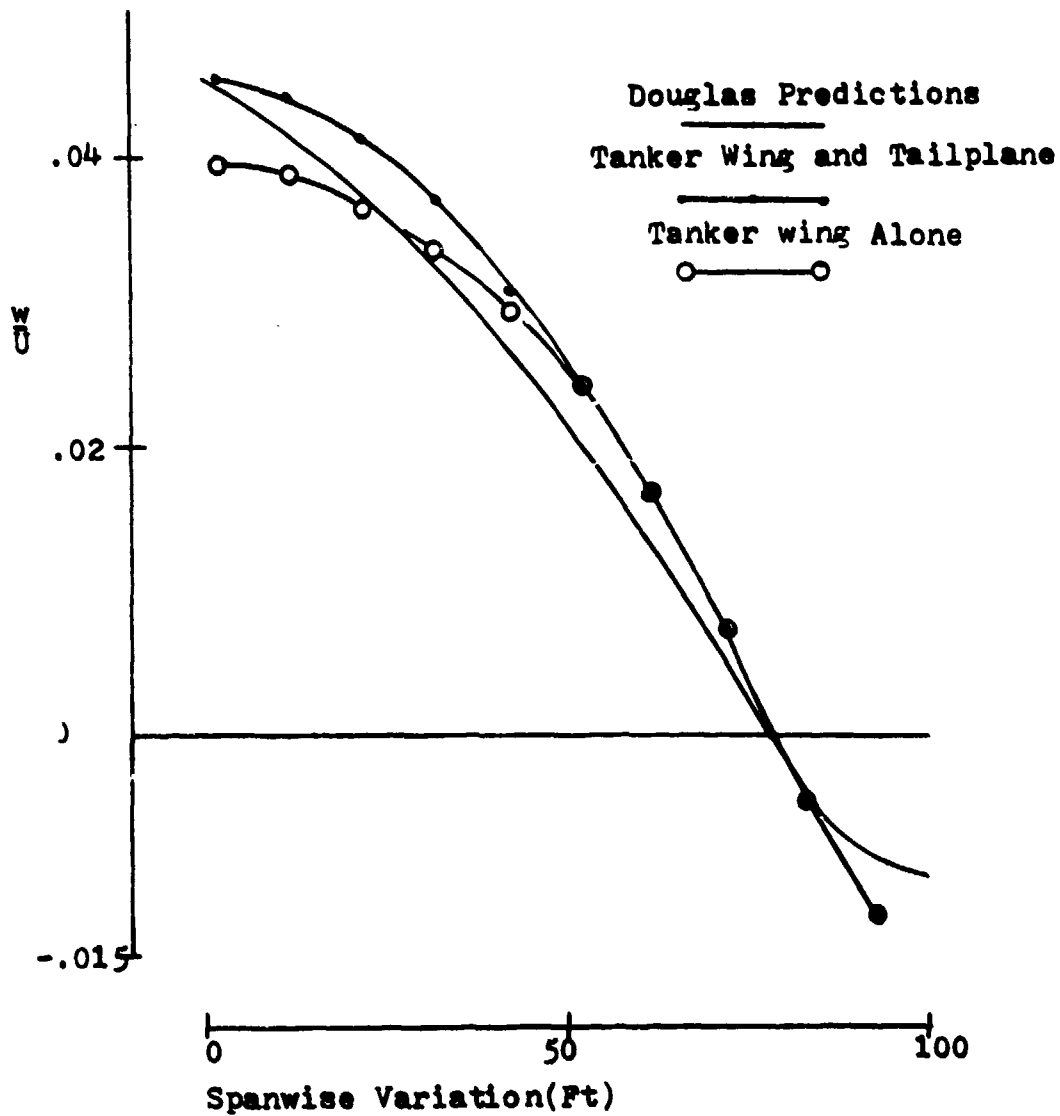


Fig. 20. Induced Downwash vs Span Position

KC-10 Data
 $\alpha = 2.3^\circ$
 Tailplane $\alpha = 2.3^\circ$

Position Information
 $x = 125$ Ft (Contact)
 $z = -25$ Ft

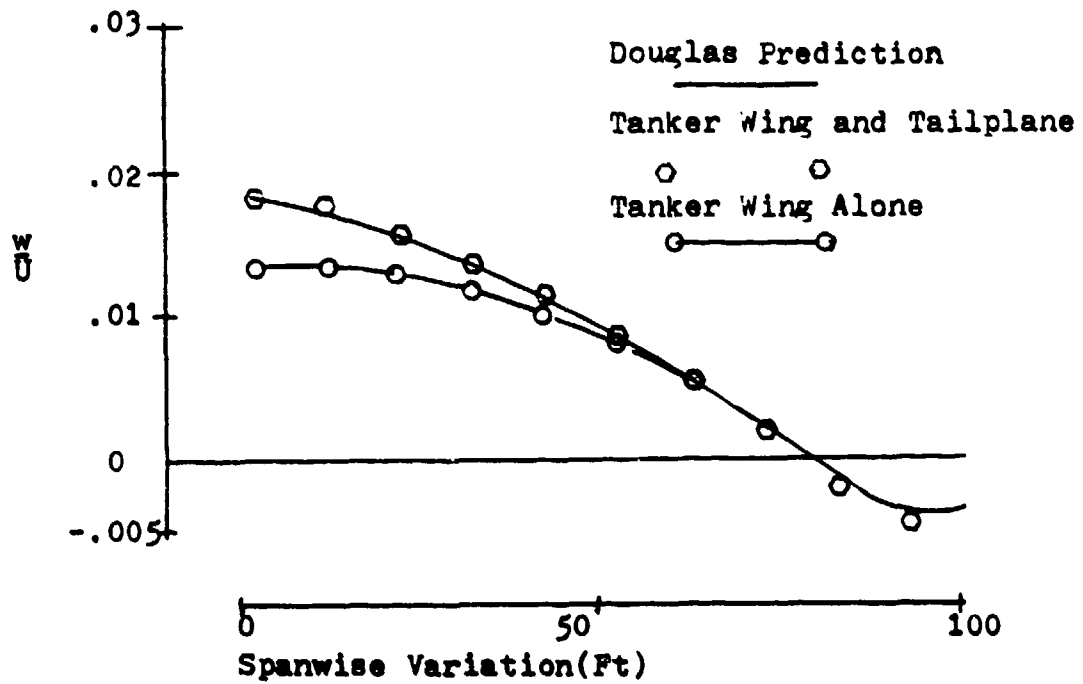


Fig. 21. Induced Downwash vs Span Position(Contact)

induced downwash, especially at a low KC-10 angle of attack. Also, tailplane effects are far less critical at points farther behind and below the KC-10.

The tailplane must be included if tanker pitching moments are required. Figure 22 indicates that the B-52 induces a significantly larger upwash on the KC-10 tailplane than on the wing. This causes a nose-down pitching moment on the tanker supporting the need for the tanker to trim nose up when the bomber moves from precontact to contact position.

When the B-52 flies behind the KC-10, the change in upwash in the tanker flowfield also causes a change in the KC-10 lift coefficient. This change is shown in Fig 23 at various distances behind and below the tanker. There is a definite increase in lift coefficient at all vertical distances when the B-52 is 125 ft behind the KC-10's wing leading edge. However, the maximum change of tanker C_L is only 2.92% of the C_L value without the B-52, indicating that the bomber wing has a minimal effect on the tanker's wing.

Considering the lift increase on the tanker wing by itself, the pilot's reaction is to slightly decrease the angle of attack to maintain level flight. However, coupled with the reaction of the tanker tailplane due to the receiver, the overall effect is a need for noseup trim to maintain level flight. The final tanker angle of attack is slightly less than the original (due to the

KC-10 Data
 $\alpha = 0.0^\circ$
Tailplane $\alpha = 0.0^\circ$
 $M = 0.6$

B-52 Data
 $\alpha = 4.0^\circ$
 $M = 0.6$

Position Information
 $x = 125$ Ft
 $z = -25$ Ft

Effect of B-52 Wing On
KC-10 Tailplane

Effect of B-52 Wing On
KC-10 Wing

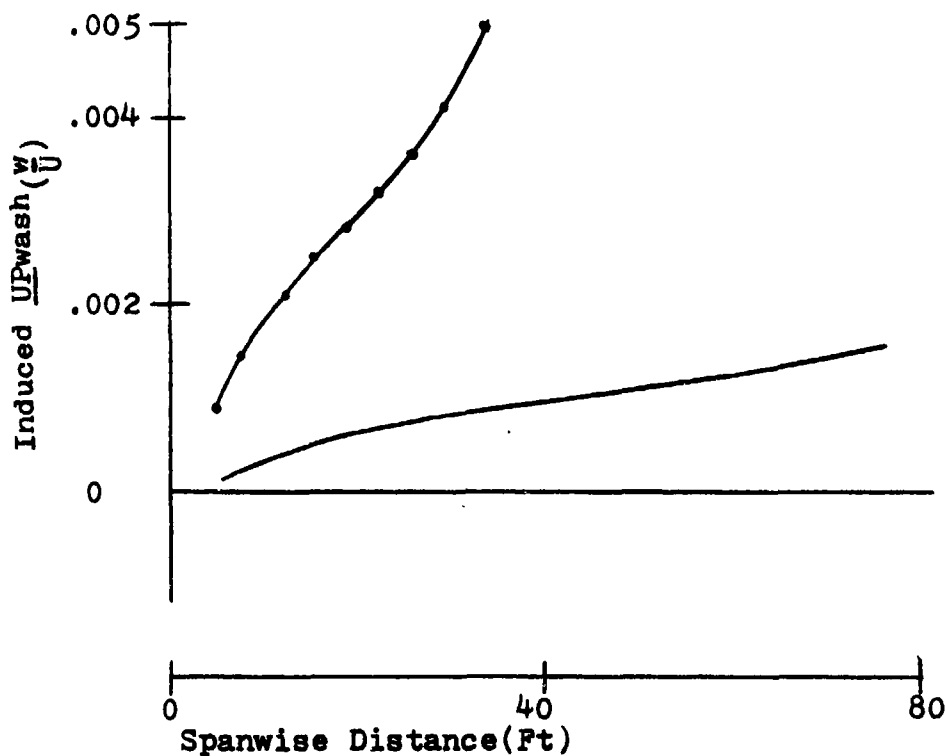


Fig. 22. Induced Upwash on the KC-10 Caused By the B-52

B-52 Data

$\alpha = 4.0^\circ$

$M = 0.6$

B-52 Vertical Position

○ — ○
z = -25 Ft

□ — □
z = -35 Ft

△ — △
z = -75 Ft

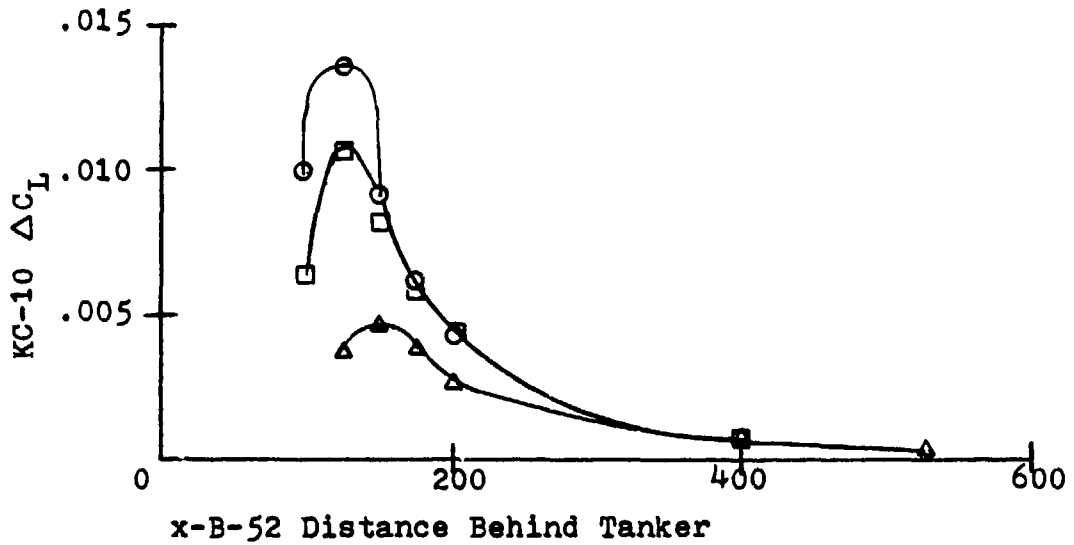


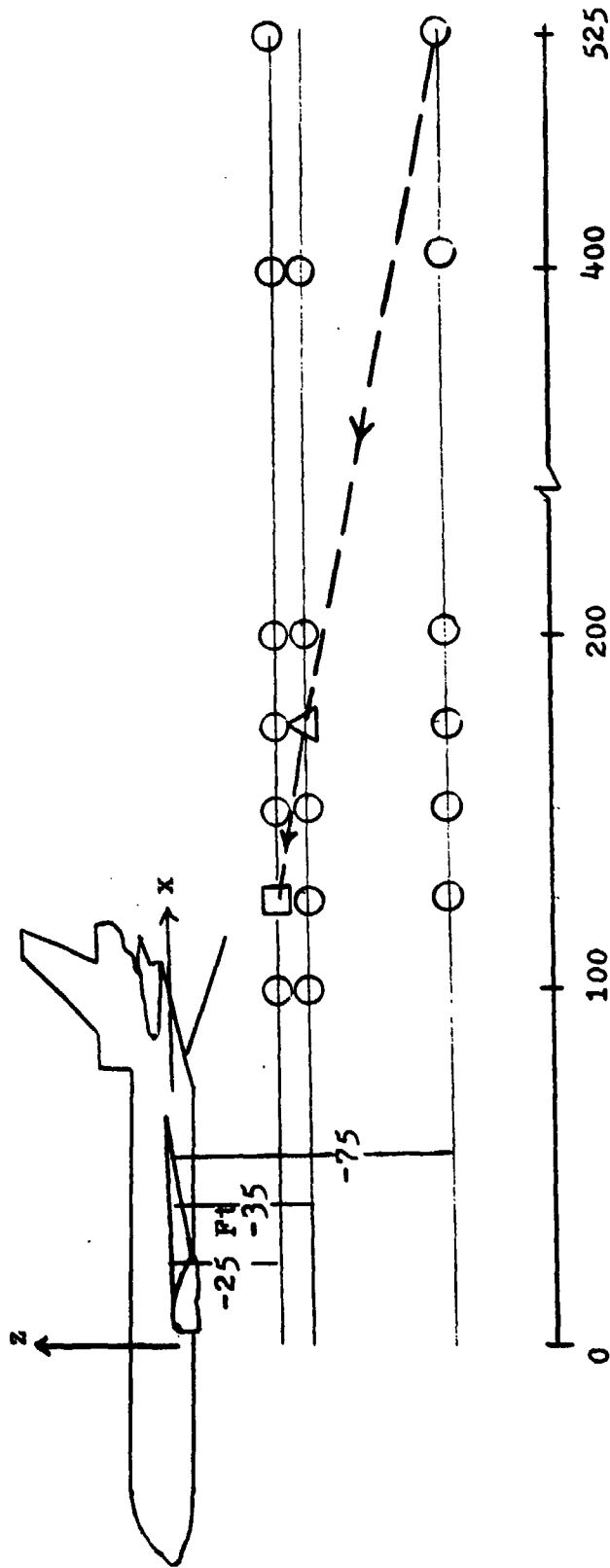
Fig. 23. Change of KC-10 Lift Coefficient vs B-52 Position

lift increase) and the need for noseup trim is due to the downward pitching caused by the receiver.

The LATEX Program was run for numerous positions behind and below the tanker. Figure 24 indicates the points checked and the dark black line is the B-52's desired flight path. The object was to determine the B-52's change in angle of attack when approaching the KC-10 and, directly related to the angle of attack, the change in the B-52 pitching moment. The results are shown on Figs 25 and 26.

Both pitching moment and angle of attack are substantially effected by the distance below the tanker (approximately 50% decrease for a 50 ft decrease in receiver altitude). This result was also expected and is justified by both the Douglas data and flight experience.

- Contact Position
 - △ Precontact Position
 - Other Positions Studied
- B-52 Flight Path



Distance B-52 Wing is Behind KC-10 Wing (Ft)

Scale 1CM=20.2Ft

Fig. 24. B-52 Positions Evaluated by VLM

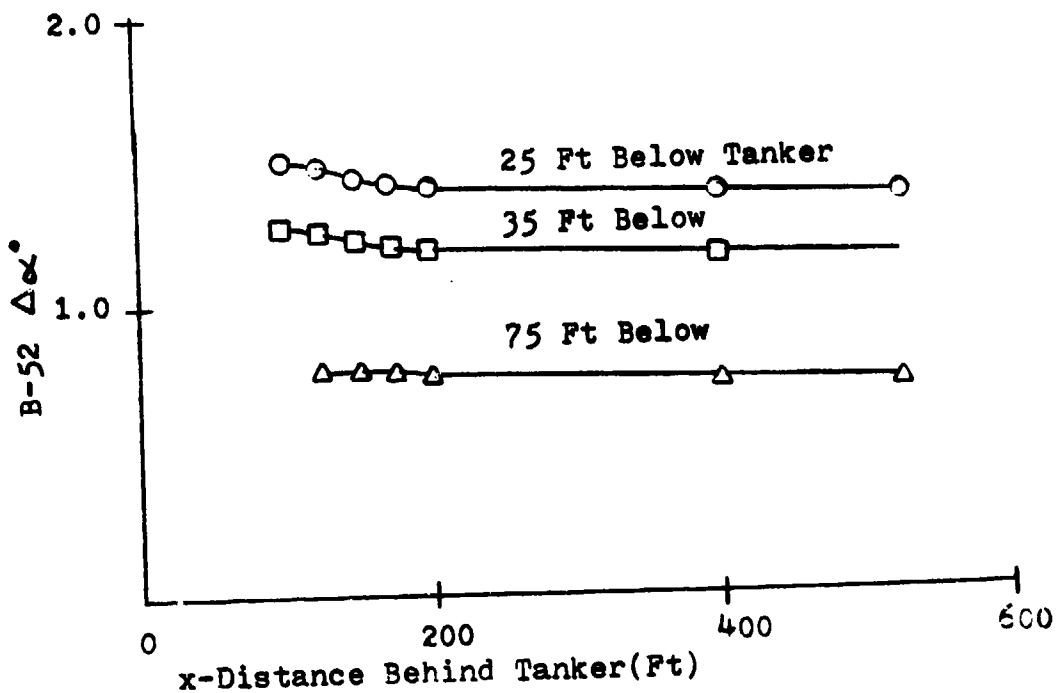


Fig. 25. Change of B-52 Angle of Attack vs B-52 Position

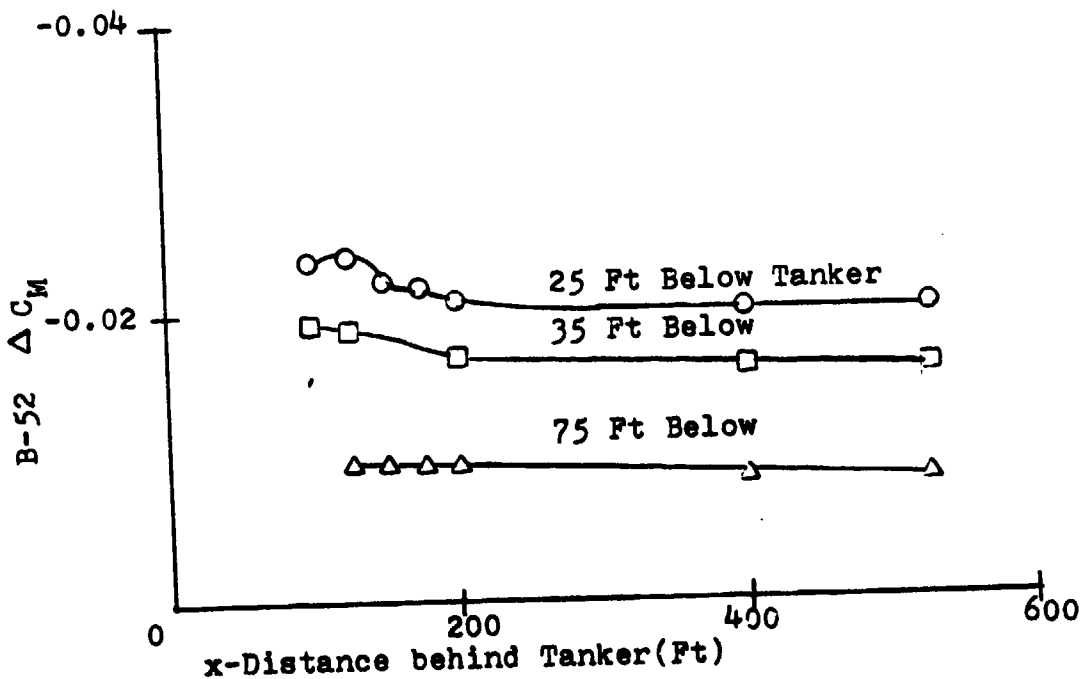


Fig. 26. Change of B-52 Pitching Moment vs B-52 Position

VI. Conclusions and Recommendations

The idea that a tanker can be represented by a linear circulation distribution and a vortex sheet or a single horseshoe vortex proved to be reasonable. Equations (2), (3), and (6) provide qualitatively accurate results for induced downwash velocity at the receiver and can be easily programmed into a hand held programmable calculator. This method is sufficient for only a few data points and is a good place to start to get an approximate idea of the flow field. It also shows that the changes in the tanker's lift distribution significantly influences the induced downwash. The analytical solution generally over-estimates the induced downwash by 25-35%, because the analytic solution uses a rectangular wing, and the downwash fields of rectangular and swept wings differ (8).

The Vortex Lattice approach provides a more accurate method that is capable of predicting not only the induced downwash, but also the change in receiver angle of attack, change of the receiver pitching moment, and change in the tanker lift coefficient.

Other areas of interest were also studied. The comparison of rectangular vs swept wings indicated that the actual swept wing model provides a closer estimation of induced downwash and should be used in air refueling evaluation. The overall effect of the tanker tailplane

on the bomber was found to be relatively small (less than 10% change in induced downwash), especially with the receiver well below the tanker.

Comparison of the results of LATEX and Douglas data was found to be very good (See Figs 19, 20, 21), especially at lower tanker angles of attack. The trends and magnitudes of the change in the receiver's angle of attack and pitching moment, and change in tanker lift, were in the proper direction and reasonable based on flight experience.

LATEX is capable of matching Douglas predictions of induced downwash within 5-10%, by representing the tanker and receiver aircraft by flat plate planforms. Results indicate that the VLM may provide the majority of information necessary for evaluating air refueling aerodynamics. However, the total error caused by using VLM or any computer prediction will not be realized without wind tunnel and/or flight test data.

A number of assumptions were made in this study. These include neglecting effects of the fuselages, wing camber, and wake roll up. Effects of out of symmetry plane approaches on the receiver rolling moment were also not treated.

Fuselage effects may have a significant influence on the pitching moments of both the receiver and the tanker. The fuselage may also vary the downwash flowfield by interrupting the downwash caused by the wings. The results of a computer analysis with and without the tanker

fuselage should be compared with the results obtained here to determine the importance of modeling the fuselage. Wind tunnel tests would also prove beneficial. They would give more credibility to both the contractor data and the LATEX results and also give a better idea of what actually happens to the flow behind the tanker.

Another area of investigation is to study the effects of camber. The LATEX program needs to be modified to permit treatment of cambered wings. This would determine if a flat plate wing is a good assumption.

A more accurate representation of the tanker's wake could also be modeled. Wind tunnel tests are necessary to determine the location of the wake, then a computer model could be developed to simulate the wake.

A final area to investigate is the receiver rolling moment changes when approaching the tanker. This area is critical for a realistic simulation, because it is a problem area for many student pilots. It may be possible to modify LATEX to provide the information that is needed.

By accomplishing these studies, the total potential of using a vortex lattice method to model air refueling between a tanker and heavy receiver would be realized.

Appendix A

Velocity Field Induced by a Linear Lifting Line and a Semi-Infinite Sheet at Any Point in Space

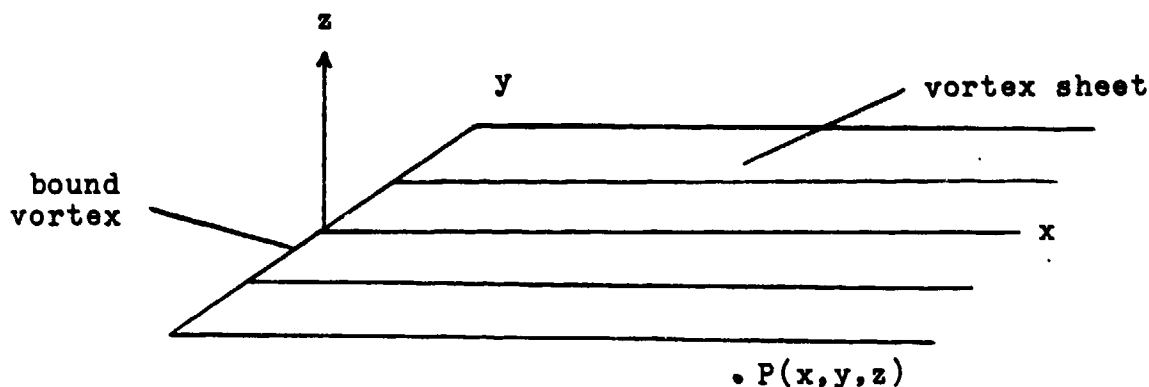


Fig. 27. Sketch of Assumed Tanker

The velocity induced at point P is caused by the bound vortex (lifting line) located on the y axis and a planar vortex sheet issuing from the bound vortex. The sheet is located in the x-y plane and all vortex legs are parallel to the x axis. The effect due to the bound vortex will be considered first.

The induced velocity (\bar{V}) at P due to a vortex filament segment $d\bar{l}$ from (1) is:

$$d\bar{V}_{\ell\ell} = \frac{\Gamma_{\ell\ell}(y^1)(d\bar{l} \times \bar{r})}{4\pi r^3} \quad (9)$$

where \bar{r} is a vector from dl to P. The $\ell\ell$ subscript refers to the lifting line.

In this case:

$$d\bar{\ell} = dy\bar{j} \quad r = x\bar{i} + (y-y^1)\bar{j} + z\bar{k}$$

therefore:

$$d\bar{\ell} \times d\bar{r} = -\bar{k}x dy^1 + \bar{j}z dy^1$$

$$r^3 = \{x^2 + (y-y^1)^2 + z^2\}^{3/2}$$

x^1, y^1, z^1 indicates the coordinate on the vortex

Substituting in to (9):

$$dV_{\ell\ell} = \frac{\bar{i} \Gamma_{\ell\ell}(y^1) z dy^1}{4\pi \{x^2 + (y-y^1)^2 + z^2\}^{3/2}} - \frac{\bar{k} \Gamma_{\ell\ell}(y^1) x dy^1}{4\pi \{x^2 + (y-y^1)^2 + z^2\}^{3/2}} \quad (9a)$$

To find the total contribution of the lifting line, Eq (9a) must be integrated over the wing span, therefore:

$$dV_{\ell\ell} = \frac{\bar{i}}{4\pi} \int_{-b/2}^{b/2} \frac{\Gamma_{\ell\ell}(y^1) z dy^1}{\{x^2 + (y-y^1)^2 + z^2\}^{3/2}} - \frac{\bar{k}}{4\pi} \int_{-b/2}^{b/2} \frac{\Gamma_{\ell\ell}(y^1) x dy^1}{\{x^2 + (y-y^1)^2 + z^2\}^{3/2}} \quad (10)$$

Before proceeding, the contribution of the vortex sheet will be derived in integral form.

The vortex sheet consists of an infinite number of filaments emanating from the lifting line and extending to infinity. The strength of each filament is $\frac{d\Gamma_{\ell\ell}(y^1)}{dy^1} dy^1$

in accordance with Helmholtz' Vortex theorem (6:148).

For one filament issuing from y^1 on the lifting line, the induced velocity at P due to this filament is

$$dV_s = -\frac{d\Gamma_{\ell\ell}(y^1)dy^1}{dy^1} \frac{d\bar{\ell}x\bar{r}}{4\pi r^3} \quad (11)$$

$d\bar{\ell}$ is now a small segment on the filament and again \bar{r} is a vector from $d\bar{\ell}$ to P.

In this case:

$$\bar{r} = (x-x^1)\bar{I} + (y-y^1)\bar{J} + z\bar{K}$$

$$d\bar{\ell} = dx^1\bar{I}$$

Therefore:

$$d\bar{\ell}x\bar{r} = \bar{K}dx^1(y-y^1) - \bar{J}zdx^1$$

$$r^3 = \{(x-x^1)^2 + (y-y^1)^2 + z^2\}^{3/2}$$

Substituting into Eq (11) gives:

$$dV_s = \frac{d\Gamma_{\ell\ell}(y^1)dy^1}{dy^1 4\pi} \cdot \frac{+\bar{J}zdx^1 - \bar{K}dx^1(y-y^1)}{\{(x-x^1)^2 + (y-y^1)^2 + z^2\}^{3/2}} \quad (12)$$

The contribution of the entire filament is found by integrating Eq (12) over x^1 giving

$$d\bar{V}_s = \int_{x^1=0}^{\infty} \frac{d\Gamma_{\ell\ell}(y^1)}{dy^1} \frac{dy^1}{4\pi} \cdot \frac{+jz - K(y-y^1)}{\{(x-x^1)^2 + (y-y^1)^2 + z^2\}^{3/2}} dx^1 \quad (13)$$

Integrating Eq (13) over the span gives the equation induced velocity due to the vortex sheet. Therefore,

$$\bar{V}_s = \frac{1}{4} \int_{-b/2}^{b/2} \int_{-\infty}^{\infty} \frac{d\Gamma_{\ell\ell}(y^1)}{dy^1} \cdot \frac{+jz - K(y-y^1)}{\{(x-x^1)^2 + (y-y^1)^2 + z^2\}^{3/2}} dx^1 dy^1 \quad (14)$$

The total velocity contribution is found by adding the results of the sheet and the lifting together (Eq (10) plus Eq (14)) giving:

$$\begin{aligned} \bar{V}(x,y,z) &= \frac{j}{4\pi} \int_{-b/2}^{b/2} \frac{\Gamma(y^1) z dy^1}{\{x^2 + (y-y^1)^2 + z^2\}^{3/2}} \\ &+ \frac{j}{4\pi} \int_{-b/2}^{b/2} \int_{-\infty}^{\infty} \frac{d\Gamma(y^1) z}{dy^1 \{(x-x^1)^2 + (y-y^1)^2 + z^2\}^{3/2}} dx^1 dy^1 \\ &- \frac{K}{4\pi} \left\{ \int_{-b/2}^{b/2} \int_{-\infty}^{\infty} \frac{d\Gamma(y^1)(y-y^1)}{dy^1 \{(x-x^1)^2 + (y-y^1)^2 + z^2\}^{3/2}} dx^1 dy^1 \right. \\ &\quad \left. + \int_{-\infty}^{\infty} \frac{\Gamma(y^1)x}{\{x^2 + (y-y^1)^2 + z^2\}^{3/2}} dy^1 \right\} \quad (15) \end{aligned}$$

Integrating over x^1 yields equations of the following form:

$$\int_0^{\infty} \frac{dx^1}{\{(x-x^1)^2+(y-y^1)^2+z^2\}^{3/2}} = \int_0^{\infty} \frac{dx^1}{\{(x^1)^2-2xx^1+x^2+(y-y^1)^2+z^2\}}$$

Integrating and evaluating at the limits gives:

$$\frac{1}{(y-y^1)^2+z^2} + \frac{x}{\{x^2+(y-y^1)^2+z^2\}^{1/2}\{(y-y^1)^2+z^2\}}$$

Substituting back into Eq (14) yields:

$$\begin{aligned} V(x,y,z) &= \frac{\bar{I}z}{4\pi} \int_{-b/2}^{b/2} \frac{\Gamma(y^1) dy^1}{\{x^2+(y-y^1)^2+z^2\}^{3/2}} \\ &+ \frac{\bar{I}z}{4\pi} \int_{-b/2}^{b/2} \frac{d\Gamma(y^1)}{dy^1} \frac{x+\{x^2+(y-y^1)^2+z^2\}^{1/2}}{\{(y-y^1)^2+z^2\}\{x^2+(y-y^1)^2+z^2\}^{1/2}} dy^1 \\ &- \frac{\bar{K}}{4\pi} \left\{ \int_{-b/2}^{b/2} \frac{(y-y^1) d\Gamma(y^1)}{dy^1} \left[\frac{1}{(y-y^1)^2+z^2} + \frac{x}{\{x^2+(y-y^1)^2+z^2\}^{1/2}\{(y-y^1)^2+z^2\}} \right] \right. \\ &\quad \left. + x \int_{-b/2}^{b/2} \frac{\Gamma(y^1)}{\{x^2+(y-y^1)^2+z^2\}^{3/2}} dy^1 \right\} \end{aligned}$$

Before integrating, it is necessary to choose a value for Γ . A common choice is to assume an elliptical circulation distribution where:

$$\Gamma(y^1) = \Gamma_0 \left(1 - (y^1/b)^2\right)^{\frac{1}{2}}$$

$$\frac{d\Gamma(y^1)}{dy^1} = \frac{-\Gamma_0 (y^1/b)}{\left(1 - (y^1/b)^2\right)^{\frac{1}{2}}}$$

Unfortunately, if an elliptical distribution is used, Eq (16) is not analytically integrable. Therefore, to keep the problem analytical, linear circulation distributions were chosen.

The first to be considered is a tent circulation distribution (Fig 28).

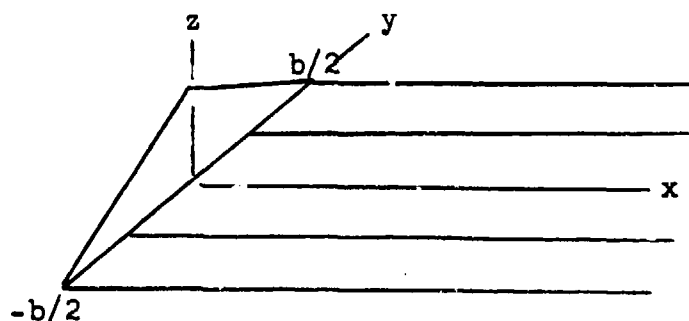


Fig. 28 Tanker Represented by Tent Circulation Distribution

In equation form,

$$\Gamma_t = \begin{cases} \Gamma_0 (1 - y^1/b), & 0^+ \leq y^1 \leq b \\ \Gamma_0 (1 + y^1/b), & -b \leq y^1 \leq 0^- \end{cases}$$

When these values are substituted into Eq (16), all integrals can be put in standard form and be integrated.

Substituting the linear form of Gamma into Eq (16) the induced velocity in the x direction (u) becomes

$$u = \frac{\Gamma_o z}{4\pi} \int_{-b/2}^{0^-} \frac{(1+y^1/b)dy^1}{\{R+(y^1)^2-2yy^1\}^{3/2}} + \int_0^{b/2} \frac{(1-y^1/b)dy^1}{\{R+(y^1)^2-2yy^1\}^{3/2}} \quad (17)$$

Integrating Eq 17 yields:

$$u = \frac{2\Gamma_o}{4\pi(x^2+z^2)} \left\{ \frac{b/2-2y+2R/b}{(R-yb+b^2/4)^{3/2}} + \frac{b/2+2y+2R/b}{(R+yb+b^2/4)^{3/2}} - \frac{4R}{b(R)^{3/2}} \right\} \quad (18)$$

Again, substituting the linear form of Gamma into Eq (16) the induced velocity in the y direction (V_y) becomes:

$$v = \frac{z}{4\pi} \int_{-b/2}^{0^-} \frac{2\Gamma_o dy^1}{b\{(y-y^1)^2+z^2\}} - \int_0^{b/2} \frac{2\Gamma_o dy^1}{b\{(y-y^1)^2+z^2\}} \\ + \int_{-b/2}^{0^-} \frac{2\Gamma_o x dy^1}{b\{x^2+(y-y^1)^2+z^2\}^{3/2}\{(y-y^1)^2+z^2\}} - \int_0^{b/2} \frac{2\Gamma_o x dy^1}{b\{x^2+(y-y^1)^2+z^2\}^{3/2}\{(y-y^1)^2+z^2\}} \quad (19)$$

Integrating Eq (19) yields:

$$\begin{aligned}
v = \frac{\Gamma_o}{2\pi b} & \left[2 \tan^{-1} (y/z) - \tan^{-1} \frac{b/2-y}{z} + \tan^{-1} \frac{b/2+y}{z} \right. \\
& - 2 \tan^{-1} \frac{y}{(x^2+y^2+z^2)^{1/2}} - \tan^{-1} \frac{(y+b/2)}{\{(y+b/2)^2+x^2+z^2\}^{1/2}} \\
& \left. + \tan^{-1} \frac{(y-b/2)}{\{(y-b/2)^2+x^2+z^2\}^{1/2}} \right] \quad (20)
\end{aligned}$$

Finally, to find the induced velocity in the z direction (downwash) substituting Gamma into Eq (16) gives:

$$\begin{aligned}
w = \frac{-1}{4\pi} & \left[\frac{2\Gamma_o}{b} \int_{-b/2}^{0^-} \frac{(y-y^1) dy^1}{(y-y^1)^2+z^2} - \frac{2\Gamma_o}{b} \int_{0^+}^{b/2} \frac{(y-y^1) dy^1}{(y-y^1)^2+z^2} \right. \\
& + \frac{2\Gamma_o x}{b} \int_{-b/2}^{0^-} \frac{(y-y^1) dy^1}{\{x^2+(y-y^1)^2+z^2\}^{3/2} \{(y-y^1)^2+z^2\}} \\
& - \frac{2\Gamma_o x}{b} \int_0^{b/2} \frac{(y-y^1) dy^1}{(y-y^1)^2+z^2} + x\Gamma_o \int_{-b/2}^{b/2} \frac{(1+y^1/b) dy^1}{\{x^2+(y-y^1)^2+z^2\}^{3/2}} \\
& \left. + x\Gamma_o \int_0^{b/2} \frac{(1-y^1/b) dy^1}{\{x^2+(y-y^1)^2+z^2\}^{3/2}} \right] \quad (21)
\end{aligned}$$

Integrating Eq (21):

$$\begin{aligned}
 w = \frac{-\Gamma_0}{4\pi} & \left[-\frac{1}{b} \ln \left| \frac{z^2 + y^2}{z^2 + y^2 + by + b^2/4} \right| + \frac{1}{b} \ln \left| \frac{z^2 + y^2 + b^2/4 - by}{z^2 + y^2} \right| \right. \\
 & - \frac{2}{b} \ln \left| \frac{(R)^{\frac{1}{2}} - x}{(R)^{\frac{1}{2}} + x} \right| + \frac{1}{b} \ln \left| \frac{(R + yb + b^2/4)^{\frac{1}{2}} - x}{(R + yb + b^2/4)^{\frac{1}{2}} + x} \right| \\
 & + \frac{1}{b} \ln \frac{(R - yb + b^2/4)^{\frac{1}{2}} - x + \frac{x(b/2 + 2y + 2R/b)}{(x^2 + z^2)(R + b^2/4 + yb)^{\frac{1}{2}}}}{(R - yb + b^2/4)^{\frac{1}{2}} + x} \\
 & \left. + \frac{x(b/2 - 2y + 2R/b)}{(x^2 + z^2)(R + b^2/4 - yb)^{\frac{1}{2}}} - \frac{x(4R/b)}{(x^2 + z^2)(R)^{\frac{1}{2}}} \right] \quad (22)
 \end{aligned}$$

Equation (22) gives the induced velocity in the z direction at any point in space (except $x=y=z=0$) due to a linear tent circulation distribution and its vortex sheet.

To determine the effect of tanker lift distribution on induced velocity, a modified linear circulation distribution was also evaluated.

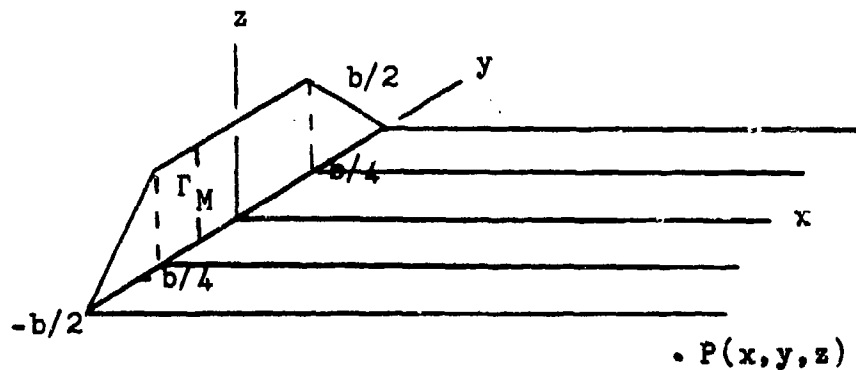


Fig. 29 Tanker Represented by Modified Linear Circulation Distribution

The only difference between the modified linear circulation distribution and the tent distribution is the value for Gamma.

In this case:

$$2\Gamma_M \left(1 + \frac{y^1}{b/2}\right) \quad -\frac{b}{2} < y^1 < -\frac{b}{4}$$

$$\Gamma(y^1) = \Gamma_M \quad -\frac{b}{4} < y^1 < \frac{b}{4}$$

$$2\Gamma_M \left(1 - \frac{y^1}{b/2}\right) \quad \frac{b}{4} < y^1 < \frac{b}{2}$$

and

$$\frac{2\Gamma_M}{b/2} \quad -\frac{b}{2} < y^1 < -\frac{b}{4}$$

$$\frac{d\Gamma(y^1)}{dy} = 0 \quad -\frac{b}{4} < y^1 < \frac{b}{4}$$

$$\frac{-2\Gamma_M}{b/2} \quad \frac{b}{4} < y^1 < \frac{b}{2}$$

Substituting these values for Gamma into Eq (16) and integrating yields:

$$u = \frac{2\Gamma_M}{(x^2+z^2)4\pi} \left[\frac{-b/2-y+4R/b}{2\{x^2+(y+b/4)^2+z^2\}^{3/2}} + \frac{b+4R/b}{\{x^2+(y+b/2)^2+z^2\}^{3/2}} \right. \\ \left. + \frac{-b/2+y+4R/b}{2\{x^2+(y-b/4)^2+z^2\}^{3/2}} + \frac{b+4R/b}{\{x^2+(y-b/2)^2+z^2\}^{3/2}} \right] \quad (23)$$

$$\begin{aligned}
v = & \frac{\Gamma_M}{\pi b} \left[\tan^{-1} \frac{b/2-2y}{2z} - \tan^{-1} \frac{-b-2y}{2z} - \tan^{-1} \frac{b-2y}{2z} \right. \\
& + \tan^{-1} \frac{b/2-2y}{2z} - \frac{1}{2} \tan^{-1} \frac{y+b/4}{\{x^2+(y+b/4)^2+z^2\}^{\frac{1}{2}}} \\
& - \frac{1}{2} \tan^{-1} \frac{y-b/4}{\{x^2+(y-b/4)^2+z^2\}^{\frac{1}{2}}} + \frac{1}{2} \tan^{-1} \frac{y+b/2}{\{x^2+(y+b/2)^2+z^2\}^{\frac{1}{2}}} \\
& \left. + \frac{1}{2} \tan^{-1} \frac{y-b/2}{\{x^2+(y-b/2)^2+z^2\}^{\frac{1}{2}}} \right] \quad (24)
\end{aligned}$$

$$\begin{aligned}
w = & \frac{-\Gamma_M}{4\pi} \left[\frac{-\frac{4x}{b} - 2xy - \frac{4Rx}{b}}{(x^2+z^2)\left(\frac{b^2}{16} + \frac{yb}{2} + R\right)^{\frac{1}{2}}} + \frac{bx + 4xy + 4Rx/b}{(x^2+z^2)\left(\frac{b^2}{4} + yb + R\right)^{\frac{1}{2}}} \right. \\
& \left. - \frac{-\frac{bx}{4} - \frac{4Rx}{b} + 2xy}{(x^2+z^2)\left(\frac{b^2}{16} - \frac{yb}{2} + R\right)^{\frac{1}{2}}} + \frac{bx - 4xy + 4\frac{Rx}{b}}{(x^2+z^2)\left(\frac{b^2}{4} - yb + R\right)^{\frac{1}{2}}} \right. \\
& - \frac{2}{b} \ln \left| \frac{y^2+z^2+b^2/16+yb/2}{y^2+z^2+b^2/4+yb} \right| + \frac{4}{b} \ln \left| \frac{y^2+z^2+b^2/4-yb}{y^2+z^2+b^2/16-yb/2} \right| \\
& - \left(\frac{2}{b}\right) \ln \frac{(R+yb/2+b^2/16)^{\frac{1}{2}} - x}{(R+yb/2+b^2/16)^{\frac{1}{2}} + x} + \frac{2}{b} \ln \frac{(R+yb+b^2/4)^{\frac{1}{2}} - x}{(R+yb+b^2/4)^{\frac{1}{2}} + x} \\
& \left. + \frac{2}{b} \ln \frac{(R-yb+b^2/4)^{\frac{1}{2}} - x}{(R-yb+b^2/4)^{\frac{1}{2}} + x} - \frac{2}{b} \ln \frac{(R-yb/2+b^2/16)^{\frac{1}{2}} - x}{(R-yb/2+b^2/16)^{\frac{1}{2}} + x} \right] \quad (25)
\end{aligned}$$

Integrals used in the derivation:

For u (Eq 17):

$$\int \frac{dy^1}{\{x^2+(y-y^1)^2+z^2\}^{3/2}} = \int \frac{dy^1}{Y^{\frac{3}{2}}} = \frac{y^1-y}{(x^2+z^2)\{(y^1)^2-2y^1y+R\}^{\frac{1}{2}}}$$

$$\int \frac{y^1 dy^1}{\{x^2+(y-y^1)^2+z^2\}^{3/2}} = \int \frac{y^1 dy^1}{Y^{\frac{3}{2}}} = \frac{yy^1-R}{(x^2+z^2)\{(y^1)^2-2yy^1+R\}^{\frac{1}{2}}}$$

For v (Eq 19):

$$\int \frac{dy^1}{\{(y-y^1)^2+z^2\}} = \int \frac{dy^1}{Y} = \frac{1}{z} \tan^{-1} \left(\frac{y^1-y}{z} \right)$$

$$\int \frac{dy^1}{\{(y-y^1)^2+z^2\}\{x^2+(y-y^1)^2+z^2\}^{\frac{1}{2}}} \quad \text{let } n=y-y^1 \quad b^2=z^2$$

$$dn=-dy^1 \quad a^2=x^2+z^2$$

Substituting

$$-\int \frac{dn}{\{n^2+b^2\}\{n^2+a^2\}^{\frac{1}{2}}} = \frac{1}{b(a^2-b^2)^{\frac{1}{2}}} \tan^{-1} \frac{n(a^2-b)^{\frac{1}{2}}}{b(n^2-a^2)^{\frac{1}{2}}}$$

For w (eq 21):

$$\int \frac{(y-y^1)dy^1}{(y-y^1)^2+z^2} = -\int \frac{ndn}{n^2+z^2} = -\frac{1}{2} \ln|z^2+n^2|$$

$$\int \frac{(y-y^1)dy^1}{\{(y-y^1)^2+z^2\}\{x^2+(y-y^1)^2+z^2\}^{\frac{1}{2}}} \quad \text{let } p=(y-y^1)^2 \quad d=s^2$$

$$dp=2(y-y^1)dy^1 \quad b=x^2+z^2$$

Substituting

$$-\frac{1}{2} \int \frac{dp}{(p+d)(p+b)^{\frac{3}{2}}} = \frac{1}{2} \frac{1}{(b-d)^{\frac{3}{2}}} \ln \frac{(p+b)^{\frac{1}{2}} - (b-d)^{\frac{1}{2}}}{(p+b)^{\frac{1}{2}} + (b-d)^{\frac{1}{2}}}$$

Appendix B

Comparison of Elliptic Circulation Distribution and Linear Circulation Distributions

In order to compare the results of the various tanker circulation distributions the area under the circulation vs span curves was made equal. This in effect, caused the total lift to remain constant, even though the distribution was allowed to vary. In the equation for elliptical circulation:

$$\Gamma(y^1) = \Gamma_e \left[1 - \left(\frac{y^1}{b/2} \right)^2 \right]^{1/2} \quad -\frac{b}{2} < y^1 < \frac{b}{2} \quad (26)$$

$$\Gamma_e = \frac{4L}{\pi \rho U b} \quad (27)$$

where Γ_e is constant for each flight condition.

For the tent distribution

$$\Gamma(y^1) = \begin{cases} \Gamma_t \left(1 + \frac{y^1}{b/2} \right) & -\frac{b}{2} < y^1 < 0 \\ \Gamma_t \left(1 - \frac{y^1}{b/2} \right) & 0 < y^1 < \frac{b}{2} \end{cases} \quad (28)$$

By integrating Eqs 26 and 28 over the wing span and equating the results, a value for Γ_t can be determined.

Equation (26) will be integrated first.

$$\int_{-b/2}^{b/2} \Gamma(y^1) dy^1 = \int_{-b/2}^{b/2} \Gamma_e \left\{ 1 - \left(\frac{y^1}{b/2} \right)^2 \right\}^{\frac{1}{2}} dy^1$$

$$= \frac{2\Gamma_e}{b} \int_{-b/2}^{b/2} \{b^2/4 - (y^1)^2\}^{\frac{1}{2}} dy^1$$

where

$$\int_{-b/2}^{b/2} \{b^2/4 - (y^1)^2\}^{\frac{1}{2}} dy = \frac{1}{2} \left(y^1 \{b^2/4 - (y^1)^2\}^{\frac{1}{2}} + \frac{b^2}{4} \sin^{-1} \frac{y}{b/2} \right)_{-b/2}^{b/2}$$

$$= \frac{1}{2} \left\{ \left(0 + \frac{\pi b^2}{8} \right) - \left(0 - \frac{\pi b^2}{8} \right) \right\}$$

$$= \frac{\pi b^2}{8}$$

Therefore

$$\int_{-b/2}^{b/2} \Gamma(y^1) dy^1 = \frac{\Gamma_e \pi b}{4} \quad (29)$$

for an elliptical distribution.

Now integrate Eq (26) for the tent distribution

$$\int_{-b/2}^{b/2} \Gamma(y^1) dy^1 = \int_{-b/2}^0 \Gamma_t \left(1 + \frac{y^1}{b/2} \right) dy^1 + \int_0^{b/2} \Gamma_t \left(1 - \frac{y^1}{b/2} \right) dy^1$$

$$= \Gamma_t (b/2) \quad (30)$$

Equating Eqs (29) and (30) ensures the total circulation and lift is constant

$$\frac{\Gamma_e b \pi}{4} = \frac{\Gamma_t b}{2}$$

Solving for Γ_t

$$\Gamma_t = \frac{\Gamma_e \pi}{2} \quad (31)$$

Substituting Eq (27) for Γ_e in Eq (31) results in a functional form for Γ_t .

Thus, for the tent distribution:

$$\Gamma_t = \frac{2L}{\rho U b} \quad (32)$$

The same approach was used for both the modified circulation distribution and the horse vortex where

$$\Gamma_M = \frac{4L}{3\rho U b} \quad (33)$$

$$\Gamma_H = \frac{L}{\rho U b} \quad (34)$$

Using Eqs (32), (33), and (34) for functional forms of circulation, caused the total lift to be constant. This allows direct comparison of the results of the equations in Chapter III.

Appendix C

Operation of the LATEX Program

Background

The LATEX program originated at Rockwell International and was called Unified Vortex Lattice. It was modified repeatedly by ASD/XRHI at Wright-Patterson AFB for their particular needs. One of these modifications, called LATEX IV, was used for evaluation in this report. LATEX was run on a VAX/UNIX computer system at the Air Force Institute of Technology. The average turn around time (from Input to Output) was about 2 minutes. The remainder of this appendix consists of a brief user guide that describes how to build an input file and also how to interpret the output file.

Data Input

Input data for LATEX is accomplished by a properly formatted file. Formatting information is found on Figs 30-32 and a sample input file is found on Fig 33. The following is a brief discussion on how to set up an input file.

The first entry contains alphanumeric title information. Data input starts with line number 1 in the 12th column. Line numbers are left justified and go in columns 10, 11, and 12. All other data is right justified and

LATEX Formatting Information

<u>Line Number</u>	<u>Column Number</u>	<u>Description</u>
1	12	Alpha-numeric Title Card
	14	Mach Number
	25	Geometric Indicator 0.0 Calc. Sym. Geom(α) 1.0 Calc. Total Geom(ϕ)
	37	Matrix A Indicator 0.0 Calc. New A Matrix
	49	Print Indicator 2.0
5	12	
	14	α -Angle of Attack for the system(degrees)
	25	ϕ -Angle of Yaw(degrees)
	37	P -Roll Rate
	49	Q -Pitch Rate
	61	R -Yaw Rate
10	11	
	14	A -Reference Area
	25	\bar{c} -Reference Length
	37	x coordinate of center of gravity
	49	y coordinate of center of gravity
	61	z coordinate of center of gravity

Fig.30

Line Number	Column Number	Description
15	11	b-Span
	14	Relative Location of Alpha table
	25	RLA 0.0-Program will Ignore Alpha Table
	37	RLT-Relative Location of Twist Table
20	11	NC -Number of Components
	14	RL1 -Relative Location of Comp. #1
	25	Data \geq 50
	37	RL2
	49	RL3
	61	RL4
50	11	Component Number Identifier
	14	Symmetry Indicator 0.0 Image sym. load
	25	NI -Number of Chordwise Vortices
	37	NK -Number of Spanwise Vortices
	49	NP -Number of Elements
	61	

Fig. 31. Formatting Information(cont.)

<u>Line Number</u>	<u>Column Number</u>	<u>Description</u>
55	11	RL1 \rightarrow 5
	14	x ₁ -x coordinate
	25	y ₁ -y coordinate
	37	z ₁ -z coordinate
	49	c ₁ -chord
201	61	NKP -Number of spanwise vortices in panel 1
	10	Relative Location of twist table
	14,25,...	Twist value of each spanwise panel(radians)
	1	Minus sign(-) for line of last data input
Next line		Alpha-numeric line
Next line	1	Minus sign(-)
	12	1
	14	Mach Number(Same as in line 1)
Next line		
	5	1
	10	1

Fig.32. Formatting Information(cont.)

starts in columns 14, 25, 37, 49, and 61. For example in Fig 33, line 1; starting in column 14 is the mach number 0.6, starting in column 25 is 0.0 meaning symmetric geometry, 0.0 starting in column 37 means a new A matrix is calculated, 2.0 starting in column 49 prints out the information needed for the air refueling problem, and column 61 is not used. Line 15, columns 37-40 have a 201, indicating the twist table starts at line 201. The twist table can be used to change the angle of attack of one or all of the lifting surfaces and will be discussed later. In line 20, the 4 indicates there are 4 lifting surfaces. The 50, 100, 150, 175 are the relative location of the data for each lifting surface. In this case the KC-10 wing starts at 50, the B-52 wing starts at 100, the B-52 tailplane starts at 150, and the KC-10 tailplane starts at 175. Lines 50-70 are information about the KC-10 wing. In line 50 the 1 in column 14 means the KC-10 wing is lifting surface. The 0.0 in columns 25-27 means a symmetrical image is calculated. The 1.0 in columns 37-39 means there is one chordwise panel and the 10. in columns 49-51 means there are 10 span wise panels. The 3.0 in columns 61-63 means the KC-10 wing is broken up into 3 sections or elements (Fig 34).

The twist table starts at 201 and goes to 236 (or higher if required). The twist table can change any span wise panel angle of attack by changing its boundary condition. Inputs must be in radians and a minus input corre-

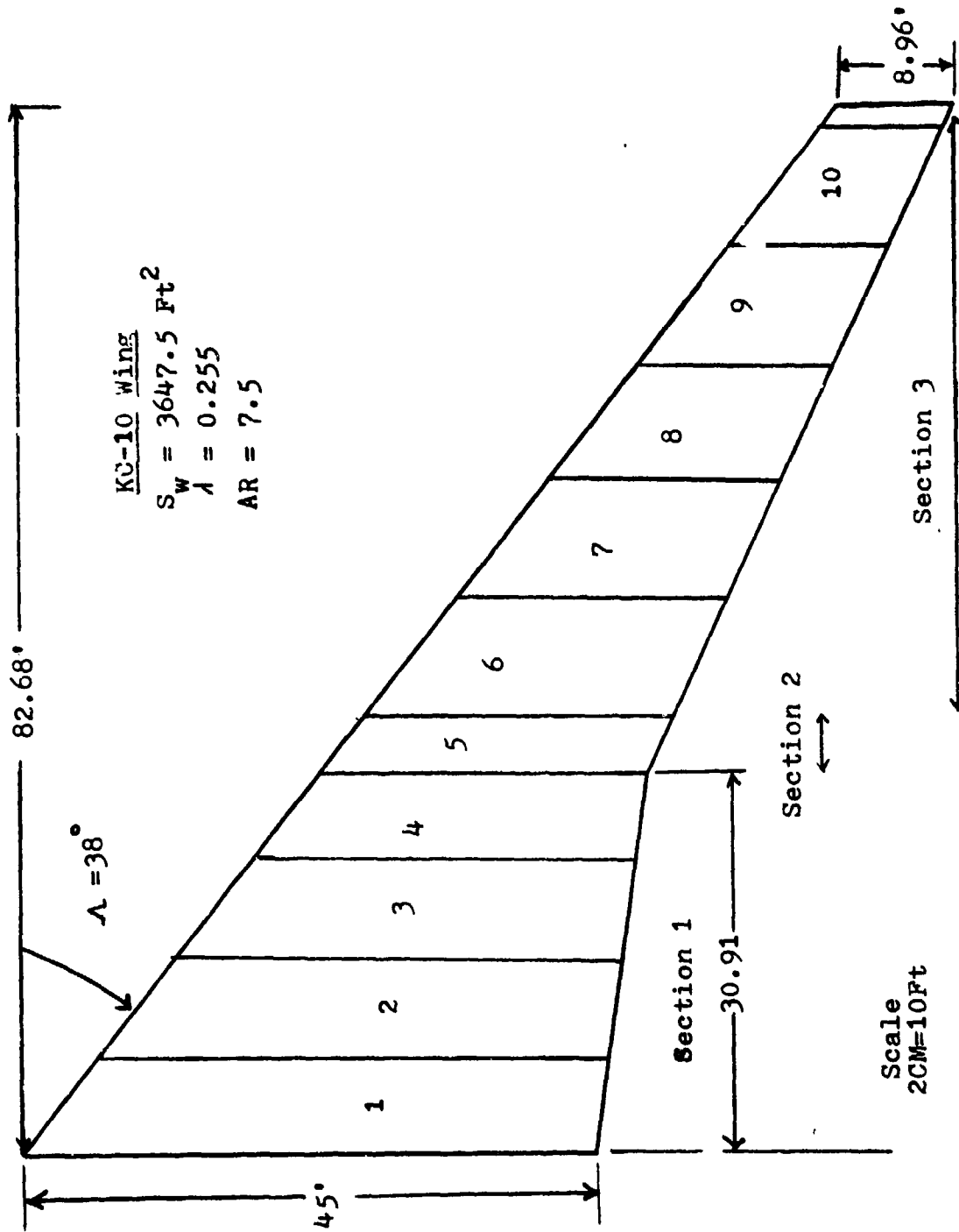


Fig. 34. Panelling Used For KC-10 Wing

sponds to a positive angle of attack. In Fig 33 lines 201 and 206 are all zeros, indicating that the twist table was not used for the KC-10 wing, therefore, it's angle of attack is 6.0° . Lines 211-231 are $-.0285$ radians (1.63°) indicate the B-52 wing angle of attack is 7.63° ($1.63^\circ + 6.0^\circ$). The B-52's tailplane AOA is 3.9° ($6.0 - (.0367)(180)$) and the KC-10's tailplane AOA is 3.0° ($6.0 - (.0524)(180)$). The advantage of using the twist table is that all four lifting surfaces can be placed at different angles of attack.

The last line of data must contain a minus sign in column 1 to indicate the end of input information. In Fig 33 this occurs on line 236. The line following the last data line is another alphanumeric title card. The next line must have a minus sign in column 1 and repeat some information found in the data. In Fig 33 line 1, Mach=0.6 is repeated. The final line must have a 1 in columns 5 and 10.

The file can now be copied onto the IN file and LATEX can be run for the desired input data.

Data Output

The output for the sample input file is found on Figs 35-38. When the LATEX is run, OUTPUT is the file name for the desired output data. On Fig 35 the input information is printed. The values of XQ, YQ, and ZQ are the x,y,z location of each panel control point XQV is the

x value of the bound vortex. ΔC_p is the change of center of pressure for the back panel. ΔC_{DIIC} is the change in the panel's induced drag.

The induced normal wash at the vortex is $\frac{w}{V}$. This value is negative for downwash. Under the section "spanwise loads," Y and Z are the y,z, coordinates of the loads, c_x , c_y , and c_z are section coefficients in x,y,z direction. When the small angle approximation is made, $c_z = c_{\alpha}$. Under the section "panel parameters" in Figure 38, Panels 1, 2, and 3, represent the 3 elements in the KC-10 wing, likewise panels 4, 5 and 6 represent the 3 elements of the B-52 wing, panel 7 is the bomber tailplane and panel 8 is the tanker tailplane. To find C_L for the bomber wing, the values of c_{zp} listed by panel's 4, 5 and 6 are added together then multiplied by 2 (due to symmetry). The total parameters are for the entire system. For example, the value for c_z is found by adding all the values in the c_{sp} column and then multiply by a factor of 2.

The previous discussion, along with the sample run, should provide the information necessary to use LATEX.

VORTEX - LATTICE RESULTS		BOTH AIRCRAFT		BOTH AIRCRAFT		***	
BOMBER AOA=6.5, CONTACT						***	
***						***	
***						***	
MACH=	.688	ALPHA=	6.888				
DELTA CP							
.36423	.48644	.46284	.53723	.55524	.58781	.61754	.63964
.59898	.42863	.46687	.48962	.51886	.52948	.54783	.56529
.50357	.62261	.66864	.67898	.69478	.78422	.89848	.82468
.82526	.82784	.82795	.82799	.82187	.82735	.83683	.84828
DELTA CTC							
-.88856	.82683	.83671	.85629	.85819	.86442	.87131	.87766
-.81187	.82833	.82845	.83972	.84136	.84619	.84962	.85322
.86123	.86549	.87884	.88838	.88685	.89199	.89732	.89993
.88882	.88814	.88817	.88828	-.88864	.88885	.88818	.88847
DELTA CD1IC							
.83878	.81653	.81863	-.88883	.88886	-.88286	-.88663	-.81868
.86471	.83559	.83857	.82551	.82569	.82434	.82336	.82212
.81918	.81744	.81543	.81815	.85649	.88182	-.88422	-.81222
.88169	.88169	.88173	.88171	.88118	.88138	.88173	.88286
DELTA CXEC							
.83814	.84256	.84734	.85626	.85825	.86186	.86468	.86423
.85314	.85682	.85982	.86523	.86385	.87853	.87288	.87791
.88841	.88293	.88548	.89844	.89255	.89382	.89311	.89998
.88172	.88184	.88198	.88198	.88112	.88143	.88192	.88263
INDUCED NORMALWASH AT VORTEX							
-.88626	-.84868	-.82352	.88886	-.88811	.88487	.81873	.82426
-.86323	-.88487	-.86988	-.86218	-.85225	-.84598	-.84265	-.83644
-.83177	-.82881	-.82485	-.81494	-.88938	-.88259	.88683	.84296
-.86786	-.86267	-.86286	-.86183	-.85392	-.85844	-.84738	-.83328

Fig. 36 LATEX Sample Output(cont.)

Y	SPANWISE LOADS	CN	CX	CY	CZ	CZC/CA	CMLE	CNC/CA	XCCP
3.863	.000	.36423	.03814	.00000	.36423	.71679	-.09106	.71679	.25000
11.587	.000	.48544	.04256	.00000	.48644	.70773	-.18161	.70773	.25000
19.313	.000	.46284	.04734	.00000	.46284	.68478	-.11301	.68478	.25000
27.838	.000	.58484	.05278	.00000	.58484	.64924	-.12681	.64924	.25000
32.888	.000	.53723	.05626	.00000	.53723	.61869	-.13431	.61869	.25000
39.386	.000	.55624	.05826	.00000	.55624	.60799	-.13986	.60799	.25000
48.518	.000	.58781	.06156	.00000	.58781	.53742	-.14636	.53742	.25000
57.738	.000	.61764	.06468	.00000	.61764	.47647	-.16441	.47647	.25000
66.942	.000	.63964	.06698	.00000	.63964	.48218	-.18991	.48218	.25000
76.154	.000	.61335	.06423	.00000	.61335	.29797	-.18334	.29797	.25000
2.461	-26.000	.39898	.06314	.00000	.39898	.54781	-.09792	.54781	.25000
7.383	-26.000	.42853	.05582	.00000	.42853	.55587	-.10512	.55587	.25000
12.386	-26.000	.44386	.05982	.00000	.44386	.56116	-.11876	.56116	.25000
17.227	-26.000	.46687	.06289	.00000	.46687	.56543	-.11662	.56543	.25000
22.149	-26.000	.48962	.06523	.00000	.48962	.56787	-.12241	.56787	.25000
26.796	-26.000	.51886	.06886	.00000	.51886	.56777	-.12771	.56777	.25000
31.169	-26.000	.52948	.07853	.00000	.52948	.56548	-.13236	.56548	.25000
35.542	-26.000	.54783	.07298	.00000	.54783	.56138	-.13696	.56138	.25000
44.287	-26.000	.56629	.07544	.00000	.56629	.55563	-.14167	.55563	.25000
48.668	-26.000	.58484	.07791	.00000	.58484	.54845	-.14621	.54845	.25000
53.632	-26.000	.60357	.08841	.00000	.60357	.53988	-.15089	.53988	.25000
57.486	-26.000	.62261	.08293	.00000	.62261	.52971	-.15563	.52971	.25000
61.778	-26.000	.64161	.08648	.00000	.64161	.51812	-.16048	.51812	.25000
66.158	-26.000	.66064	.08881	.00000	.66064	.50481	-.16516	.50481	.25000
68.523	-26.000	.67888	.09844	.00000	.67888	.48928	-.16973	.48928	.25000
74.896	-26.000	.69478	.09255	.00000	.69478	.47851	-.17367	.47851	.25000
79.268	-26.000	.70422	.09382	.00000	.70422	.46538	-.17686	.46538	.25000
83.641	-26.000	.69892	.09311	.00000	.69892	.41268	-.17473	.41268	.25000
88.814	-26.000	.65848	.08771	.00000	.65848	.36817	-.16468	.36817	.25000
2.461	-38.000	.52458	.06998	.00000	.52458	.26425	-.13117	.26425	.25000
7.383	-38.000	.62525	.08172	.00000	.62525	.03157	-.08631	.03157	.25000
12.386	-38.000	.62784	.08104	.00000	.62784	.02888	-.08676	.02888	.25000
17.227	-38.000	.62795	.08198	.00000	.62795	.01777	-.08699	.01777	.25000
22.149	-38.000	.62868	.08196	.00000	.62868	.01777	-.08716	.01777	.25000
3.863	6.000	.62799	.08198	.00000	.62799	.01169	-.08788	.01169	.25000
11.587	6.000	.62187	.08114	.00000	.62187	.02583	-.08547	.02583	.25000
19.313	6.000	.62735	.08143	.00000	.62735	.02749	-.08684	.02749	.25000
27.838	6.000	.63653	.08122	.00000	.63653	.03836	-.08916	.03836	.25000
32.888	6.000	.64828	.08263	.00000	.64828	.03168	-.09127	.03168	.25000
39.386	6.000	.64638	.08243	.00000	.64638	.02392	-.09159	.02392	.25000

Fig. 37. LATEX Sample Output(cont.)

I ***** PANEL PARAMETERS *****

PANEL	CXP	CVP	CZP	ROLL	PITCH	YAW	Y/B CP
1	.01206	.00000	.11518	-.00542	.75549	.00099	.00101
2	.00133	.00000	.01271	-.00226	.07175	.00024	.17730
3	.01200	.00000	.11463	-.03400	.56010	.00355	.29650
4	.00991	.00000	.07442	-.00499	.06653	.00066	.06599
5	.02309	.00000	.17335	-.05106	-.06170	.00000	.29462
6	.00020	.00000	.00298	-.00016	-.00067	.00001	.05460
7	.00025	.00000	.00401	-.00042	.01284	.00002	.00712
8	.00003	.00000	.00049	-.00009	.00106	.00000	.17730

Z/B CP	X/C CP	Z/B CP	X/C CP	Y/B C
.13514	.00000	.00000	-6.01922	.0010
.13514	.00000	.00000	-5.53144	.1773
.00000	.00000	.00000	-4.04104	.2905
.00000	.00000	.00000	-.75959	.0669
.00000	.00000	.00000	.36640	.2945
-.02703	.00000	.00000	2.09079	.0546
.16767	.00000	.00000	-2.59906	.0071
.16767	.00000	.00000	-2.07697	.1773

E ***** TOTAL PARAMETERS *****

CX	CY	CZ	ROLL	PITCH	YAW	Y/B CP
.11777	.00000	.99714	.00000	2.69263	.00000	.00000
***** WAKE DRAG (100% SUCTION DRAG, SUBSONIC) = .03254 E = 1.13316						
***** CDI(100%) = .03254						

Z/B CP	X/C CP	Z/B CP	X/C CP	Y/B CP
.05090	.00000	.00000	-2.54407	.00000

Fig. 38. LATEX Sample Output(cont.)

Appendix D

Relationship of Aerodynamic Coefficients and Circulation (VLM)

As previously mentioned, the VLM used a number of discrete spanwise and chordwise panels to simulate a wing. For each panel, a circulation (Γ) was determined. Once Γ was known, the aerodynamic coefficients (C_ℓ, C_L, C_M) were found as shown below.

Section Lift Coefficient

From (1:113), it was shown that the section lift was found by:

$$C_\ell = \frac{\ell}{.5\rho U^2 c} \quad (35)$$

where

$$\ell = \int_0^c \rho U \gamma(s) ds \quad (36)$$

For the VLM, $\int_0^c \gamma(s) ds = \Gamma$, where Γ was the sum of all Γ 's in the chordwise strip of interest. For example, if there were 2 chordwise panels, $\Gamma = \Gamma_1 + \Gamma_2$. The section lift could then be reduced to:

$$\ell = \rho U \Gamma \quad (37)$$

Substituting Eq (37) for ℓ in Eq (35), the section lift coefficient could now be determined with known infor-

mation.

$$C_l = \frac{2\Gamma}{U_{c_{ref}}} \quad (38)$$

Lift Coefficient

Total lift for the wind was found by (1:202).

$$L = 2\rho U \sum_{n=1}^n \Gamma_n \Delta y_n \quad (39)$$

where n was the number of spanwise panels and Δy_n was the panel width.

The lift coefficient was determined by

$$C_L = \frac{L}{qS} \quad (40)$$

Substituting Eq (39) for L in Eq (40) yielded the lift coefficient for the wing.

$$C_L = \frac{4u}{S} \sum_{n=1}^n \Gamma_n \Delta y_n \quad (41)$$

Moment Coefficient

The moment caused by aerodynamic forces acting on a lifting surface was dependent on the reference axis. Specific x,y,z coordinates of the reference axis were entered into the input file. Once the reference axis was selected, the moment coefficient could then be determined by:

$$C_M = \frac{M}{qSc}$$

(42)

The moment (M) was found by multiplying the aerodynamic force by the distance away from the reference point.

Bibliography

1. Bertin, John J. and Michael L. Smith. Aerodynamics for Engineers. Englewood Cliffs, New Jersey: Prentice-Hall, Inc., (1979).
2. DeYoung, John and Walter H. Barling, Jr. "Prediction of Downwash Behind Sweptwing Airplanes at Subsonic Speed," NACA Technical Note, 3346, (Jan 1955).
3. DeYoung, John and Charles W. Harper. "Theoretical Symmetric Span Loading at Subsonic Speeds for Wings Having Arbitrary Plan Form," NACA Technical Report No. 921, (1948).
4. Diehl, Walter S. Engineering Aerodynamics. New York: The Ronald Press Company, 31-58, (1936).
5. Douglas Aircraft Company. "KC-10A Aerial Refueling System," Interface Control Document (ICD), Configuration Item Development Spec Revision A & B. Spec #ZAO15800, Long Beach, California, (26 Jan 81).
6. Durand, W.F. Aerodynamic Theory Vol II Division E. Pasadena California: Durand Printing Committee, California Inst. of Technology, (1943).
7. Flight Manual, "B-52 G/H Flight Crew Air Refueling Procedures," T.O. 1-1C-1-15. Oklahoma City ALC/MMEDT, Tinker AFB, OK 73145.
8. Glauert, H. The Elements of Airfoil and Aircrew Theory. New York: MacMillan Company, (1944).
9. Hoeijmakers, H.W.M., and W. Voatstra. "A Higher Order Panel Method Applied to Vortex Sheet Roll-Up," AIAA Journal, 21: 516-523, (Mar 1983).
10. Kuethe, Arnold M. and Chuen-Yen Chow. Foundations in Aerodynamics: Bases of Aerodynamic Design (Third Edition), New York: John Wiley and Sons, (1976).
11. Kurlylowich, G. "A Method for Assessing the Impact of Wake Vortices on USAF Operations," Technical Report AFFDL-TR-79-3060, (Jul 1979).
12. Millikan, Clark B. "An Extended Theory of Thin Airfoils and its Application to the Biplane Problem," NACA Technical Report No. 362: 637-667, (1930).

13. Munk, Max M. "General Biplane Theory," NACA Report 151: 473-493, (1922).
14. Muttray, H. "Investigation of the Amount of Downwash Behind Rectangular and Elliptical Wings," NACA Technical Memorandum No. 787.
15. NASA Langley Research Center, Vortex-Lattice Utilization, Workshop, Hampton VA., (17-18 May 1976), (NASA-SP-405).
16. Pope, Alan. Basic Wing and Airfoil Theory, New York: McGraw Hill, (1951).
17. Spreiter, John R. and Alvin E. Sacks. "The Rolling Up of the Trailing Vortex Sheet and its Effect on the Downwash Behind Wings," The Journal of Aeronautical Sciences, 21-32, (Jan 1957).
18. Von Mises, Richard. Theory of Flight, New York: McGraw Hill Book Company, (1944).

VITA

Captain Eric H. Hoganson was born on 25 June 1953 in Burlington, Wisconsin. He attended Burlington High School and graduated in 1971. He then went to the United States Air Force Academy where he was a member of the Parachute Team. After receiving a Bachelor of Science degree in Aeronautical Engineering in 1975, he went to Undergraduate Pilot Training at Craig AFB, Alabama. Upon completion of Pilot Training he went to Seymour Johnson AFB in North Carolina where he served as Pilot and Flight Instructor with the 51st Bomb Squadron. He entered the School of Engineering, Air Force Institute of Technology, in June 1982. He married Tawnie Smalenberg from Oscoda Michigan and has a daughter named Bethany.

Permanent address: 249 E. Highland Ave.
Burlington, Wisconsin

Unclassified

SECURITY CLASSIFICATION OF THIS PAGE

REPORT DOCUMENTATION PAGE

1. REPORT SECURITY CLASSIFICATION Unclassified		1b. RESTRICTIVE MARKINGS	
2a. SECURITY CLASSIFICATION AUTHORITY		3. DISTRIBUTION/AVAILABILITY OF REPORT Approved for public release; distribution unlimited.	
2b. DECLASSIFICATION/DOWNGRADING SCHEDULE			
4. PERFORMING ORGANIZATION REPORT NUMBER(S) AFIT/GAE/AA/83D-8		5. MONITORING ORGANIZATION REPORT NUMBER(S)	
6a. NAME OF PERFORMING ORGANIZATION School of Engineering	6b. OFFICE SYMBOL (If applicable) AFIT/ENA	7a. NAME OF MONITORING ORGANIZATION	
6c. ADDRESS (City, State and ZIP Code) Air Force Institute of Technology Wright-Patterson AFB OH 45433		7b. ADDRESS (City, State and ZIP Code)	
8a. NAME OF FUNDING/SPONSORING ORGANIZATION	8b. OFFICE SYMBOL (If applicable)	9. PROCUREMENT INSTRUMENT IDENTIFICATION NUMBER	
8c. ADDRESS (City, State and ZIP Code)		10. SOURCE OF FUNDING NOS.	
		PROGRAM ELEMENT NO.	PROJECT NO.
		TASK NO.	WORK UNIT NO.
11. TITLE (Include Security Classification) See Box 19			
12. PERSONAL AUTHOR(S) Eric H. Hoganson, M.S., Capt, USAF			
13a. TYPE OF REPORT MS Thesis	13b. TIME COVERED FROM _____ TO _____	14. DATE OF REPORT (Yr., Mo., Day) 1983, December 15-17	15. PAGE COUNT 96
16. SUPPLEMENTARY NOTATION <i>John E. Wolaver</i> John E. Wolaver Dept. for Research and Professional Development Air Force Institute of Technology (AIC) Wright-Patterson AFB OH 45433			
17. COEAT: CODES		18. SUBJECT TERMS (Continue on reverse if necessary and identify by block number)	
FIELD 20	GROUP 04	Aerial Refueling, Vortex Lattice Method, KC-10, B-52, Interference Effects	
19. ABSTRACT (Continue on reverse if necessary and identify by block number)			
Title: A Study of the Aerodynamic Interference Effects During Aerial Refueling			
Thesis Chairman: Michael L. Smith, Lt Col, USAF			
21. DISTRIBUTION/AVAILABILITY OF ABSTRACT UNCLASSIFIED/UNLIMITED <input type="checkbox"/> SAME AS RPT. <input type="checkbox"/> DTIC USERS <input type="checkbox"/>		20. ABSTRACT SECURITY CLASSIFICATION Unclassified	
22a. NAME OF RESPONSIBLE INDIVIDUAL Michael L. Smith, Professor		22b. TELEPHONE NUMBER (Include Area Code) 513-255-2998	22c. OFFICE SYMBOL AFIT/ENA

An analytical approach and the vortex lattice method (VLM) were used to evaluate the interference effects of aerial refueling aerodynamics. A KC-10 tanker and a B-52 receiver were selected for study; however, the method can be applied to any tanker and receiver combination. The analytical approach represented by the tanker by a lifting line followed by a semi-infinite vortex sheet. Three linear lift distributions for the tanker wing were used to evaluate how a change in the tanker's lift distribution affects the receiver's flowfield and equations were derived for the induced downwash at any point in space. Results of the analytical equations were compared with Douglas predictions and were found to over-predict the induced downwash by 25-35%. The vortex lattice method represented the tanker with flat plate planforms of the wing and tailplane. VLM results varied from Douglas predictions by 5% or less. Results indicate that the VLM can be used to determine many of the interference effects experienced during aerial refueling.